https://doi.org/10.5194/egusphere-2024-246
Preprint. Discussion started: 1 February 2024

Ice-proximal sea-ice reconstruction in Powell Basin, Antarctica since the Last Interglacial

Wee Wei Khoo[1*], Juliane Müller[1,2,3], Oliver Esper[1], Wenshen Xiao[4], Christian Stepanek[1], Paul Gierz[1], Gerrit Lohmann[1,3,5], Walter Geibert[1], Jens Hefter[1] and Gesine Mollenhauer[1,2,3]

[1]Alfred Wegener Institute, Helmholtz Centre for Polar and Marine Research, Bremerhaven, Germany
[2]Department of Geoscience, University of Bremen, Bremen, Germany
[3]MARUM - Center for Marine Environmental Sciences, University of Bremen, Bremen, Germany
[4]State Key Laboratory of Marine Geology, Tongji University, Shanghai, China
[5]Department of Environmental Physics, University of Bremen, Bremen, Germany

Correspondence: Wee Wei Khoo (wee.wei.khoo@awi.de)

ABSTRACT. In Antarctica, the presence of sea ice in front of ice shelves promotes their stability and prevents the risk of catastrophic collapse as witnessed in recent events along the Antarctic Peninsula. Investigating past ice-proximal sea-ice conditions, especially across glacial-interglacial cycles, can provide crucial information pertaining to sea-ice variability and deepen our understanding of ocean-ice-atmosphere dynamics and feedbacks. In this study, we apply a multiproxy approach, analyzing the novel sea ice biomarker $IPSO_{25}$ (a di-unsaturated highly branched isoprenoid (HBI)), open-water biomarkers (tri-unsaturated HBIs; z-/e-trienes), and the diatom assemblage and primary productivity indicators in a marine sediment core retrieved from Powell Basin, NW Weddell Sea. These biomarkers have been established as reliable proxies for reconstructing near-coastal sea ice conditions in the Southern Ocean, where the typical use of sea ice-related diatoms can be impacted by silica dissolution. Our data shed new light on the variability of sea ice since the penultimate deglaciation, ca. 145 ka before present, and reveal a highly dynamic glacial-interglacial sea-ice setting characterized by significant shifts from perennial ice cover to seasonal sea-ice cover and open marine environment.

https://doi.org/10.5194/egusphere-2024-246
Preprint. Discussion started: 1 February 2024

1 Introduction

Sea ice plays a vital role within Earth's climate system, exerting significant influence on air-sea interactions, ocean circulation and ecosystem dynamics. Its presence alters the surface albedo of the ocean through the reflectance of incoming solar radiation, thereby minimizing ocean warming (Ebert et al., 1995). Likewise, sea ice affects the atmosphere-ocean interaction by inhibiting the exchange of heat, gas and water vapor between both media (Dieckmann and Hellmer, 2010). During sea ice formation, brine rejection occurs and leads to the production of high-saline shelf water (HSSW). This dense HSSW then sinks towards the deeper ocean. Consequently, this process results in redistribution of salinity within the water column and has a profound impact on the stratification and ventilation of the ocean (Vaughan et al., 2013). For example, in a few locations in the Southern Ocean (SO), such as the Weddell Sea, the HSSW – depending on its route and mixing process – becomes the precursor of Antarctic Bottom Water (AABW), which is a major driver of the global thermohaline circulation and an important water mass that ventilates the deep ocean basins (Naveira Garabato et al., 2002; Rintoul, 2018; Seabrooke et al., 1971). Furthermore, when sea ice melts, the freshened surface water mixes with the upwelled deep water, contributing to the mode and intermediate waters in the Atlantic, Indian and Pacific sectors of the SO (Abernathey et al., 2016; Pellichero et al., 2018). Additionally, the presence of sea ice attenuates ocean swells as they travel towards the ice shelves, thus enhancing the stability of said ice shelves and impeding calving events (Greene et al., 2018; Massom et al., 2018; Robel, 2017). In this regard, any changes to the sea-ice cover can potentially alter ice-ocean-atmosphere dynamics and ocean circulation patterns. Analyses of sea ice variability over glacial-interglacial cycles, covering periods of less and more pronounced sea ice cover, can also provide valuable information pertaining to identifying potential tipping points in the ice-ocean-atmosphere system.

Presently, numerous methods are used to reconstruct past sea-ice conditions, including biogenic proxies (biomarkers, diatoms, dinoflagellate cysts, foraminifera and ostracods), geochemical and sedimentary records such as sea salt traces in ice cores and ice-rafted debris in marine sediments (de Vernal et al., 2013 and references therein). Determination of methane sulfonic acid or sea salt-derived sodium concentrations in Antarctic ice cores permits well-dated and temporally high-resolution regional sea-ice reconstructions but is often affected by other sea-ice independent factors such as atmospheric transport (Abram et al., 2013). In particular, direct proxies, originating from sea-ice dwelling microorganisms, are often preferred as they increase the reliability of sea-ice estimation (Leventer, 1998). Despite this, our understanding of past sea ice changes in the SO remains limited. The Cycles of Sea-Ice Dynamics in the Earth System working group (C-SIDE; Chadwick et al., 2019; Rhodes et al., 2019) consolidated a list of published Antarctic marine sea-ice records, as outlined in the review paper by Crosta et al. (2022). The compilation documents 20 studies on sea-ice variability during the Holocene (0-12 ka before present (BP)), 150 records detailing changes at the Last Glacial Maximum (LGM; ca. 21 ka BP or Marine Isotope Stage (MIS) 2), and 14 sea-ice records dating back to around 130 ka BP. Notably, only two records extend beyond MIS 6 (ca. 191 ka BP). Further highlighted is the lack of (paleo) sea-ice reconstructions in regions south of 60°S, especially during the Last Interglacial (LIG) and beyond. For additional information, please refer to Crosta et al. (2022). This scarcity of records is

https://doi.org/10.5194/egusphere-2024-246
Preprint. Discussion started: 1 February 2024

attributable to difficulties in recovering marine sediment cores in the polar regions that at present are still subject to heavy year-round ice cover, and a lack of continuous sedimentary records due to erosion and disturbance at the sea floor during past glaciations. Moreover, limited preservation potential of silica frustules in SO regions beyond the opal belt, in particular proximal to the continental margin, further hampers sea-ice reconstruction using diatom assemblages (Ryves et al., 2009; Vernet et al., 2019). As such, important feedback mechanisms related to the sea ice-ice shelf system, that are particularly well observed during warmer-than-present periods and throughout climate transitions, remain poorly understood. Ultimately, this lack of knowledge – on how Antarctic ice sheets/shelves respond(ed) to oceanic forcing – may disadvantage our understanding of climate models' ability to faithfully reproduce dynamics in the ocean-sea ice-ice system, and limit our confidence in future projections of the Antarctic Ice Sheet's contribution towards global sea level rise (Deconto and Pollard, 2016; Naughten et al., 2018). For instance, Holloway et al. (2016; 2017) investigated simulated Antarctic winter sea ice (WSI) distribution that best agrees with the peak $\delta^{18}O$ value recorded in multiple East Antarctic ice cores at 128 ka BP. They determined that to match the peak isotopic value, a significant reduction in WSI, equivalent to approximately half the size of pre-industrial sea-ice cover, would have occurred at 128 ka BP in the SO. Furthermore, calculations from their study also revealed differences in WSI retreat across the SO sectors. The Atlantic sector experienced the most substantial decline, relative to pre-industrial, with a reduction of 67% sea-ice extent, while the Indian and Pacific sectors decreased by 59% and 43%, respectively (Holloway et al., 2017). Despite similar LIG-WSI retreats in marine records, inconsistency with regard to the position of the sea-ice edge, in particular in the Atlantic sector, remains evident when the proposed spatial structure of the $\delta^{18}O$-agreed WSI extent is compared to published marine records. Holloway et al. (2017) and Crosta et al. (2022) opined that this discrepancy may result from the marine records (Bianchi and Gersonde, 2002; Chadwick et al., 2020; 2022) being located too far north to adequately validate the $\delta^{18}O$-agreed WSI extent. Thus, they emphasized the need for additional marine records closer to the continental margin to adequately constrain the spatial pattern of the LIG sea-ice extent.

In recent years, the use of a novel sea-ice biomarker has been found increasingly applicable as a suitable proxy for Antarctic sea-ice reconstructions (Belt et al., 2016; Smik et al., 2016). This sea-ice biomarker, a di-unsaturated C_{25} highly branched isoprenoid (HBI) alkene, introduced as an Antarctic sea-ice proxy by Massé et al. (2011), was later termed Ice Proxy for the Southern Ocean with 25 carbon atoms ($IPSO_{25}$), drawing parallel to the Arctic IP_{25} (Belt et al., 2016). $IPSO_{25}$ is a lipid molecule produced by the sympagic diatom *Berkeleya adeliensis*, which lives in the sea-ice matrix and is generally abundant during late spring and early summer (Belt et al., 2016; Riaux-Gobin and Poulin, 2004), hence, making the biomarker a good indicator for spring/summer sea ice. Furthermore, the biomarker is well-preserved in the sediment and widely identified in areas near to the Antarctic continent (for more details, see Belt, 2018; Belt et al., 2016). Nevertheless, there remains a risk of under-/ overestimating presence of sea ice when relying solely on the $IPSO_{25}$ proxy. Thus, Vorrath et al. (2019) proposed combining open-water phytoplankton markers like dinosterol or an HBI-triene with the $IPSO_{25}$ proxy, to calculate the phytoplankton-$IPSO_{25}$ index ($PIPSO_{25}$). This enhances the quantitative application of the $IPSO_{25}$ proxy. For example, in cases where the $IPSO_{25}$ concentration is minimal or absent, this may imply either

https://doi.org/10.5194/egusphere-2024-246
Preprint. Discussion started: 1 February 2024

an open ocean condition (substantiated by a high phytoplankton signal) or the presence of a perennial ice cover (evident by a low/absent phytoplankton signal). As such, the use of the $PIPSO_{25}$ proxy, proves to be a more reliable approach to distinguish contrasting sea-ice settings (Belt and Müller, 2013; Lamping et al., 2020). To substantiate this application, Lamping et al. (2021) compared $PIPSO_{25}$-derived sea-ice estimates close to the Antarctic continental margin against satellite sea-ice observations and modelled sea-ice patterns, revealing strong correlation between the proxy, observation and modelled data. Until now, the majority of HBI-based sea-ice reconstructions has focused on Holocene and deglacial/LGM time scales (Barbara et al., 2013; 2016; Denis et al., 2010; Etourneau et al., 2013; Lamping et al., 2020; Sadatzki et al., 2023; Vorrath et al., 2020, 2023) and one reconstruction dates back to the last ca. 60 ka BP (Collins et al., 2013). Yet, this tool has not been applied towards studying sea ice variability in the Antarctic during warm climates beyond the current interglacial.

Here, we fill this gap by pursuing a multiproxy approach to investigate the glacial-interglacial environmental variability in the Powell Basin, NW Weddell Sea, and provide the first continuous ice-proximal Antarctic sea-ice record covering the last ca. 145 kyrs. We present biomarker-based reconstructions of sea-ice, subsurface ocean temperature, total organic carbon (TOC) and biogenic silica ($bSiO_2$) content, as well as diatom-based sea-ice concentration (SIC) and summer sea surface temperature (SSST). This information is complemented by reconstructions of sea ice, primary productivity and SSST records from a neighboring core in the southern Scotia Sea as well as numerically-modeled sea ice, sea surface and subsurface temperatures to track latitudinal shifts in the environmental development in the Atlantic sector of the SO.

2 Study area

The Powell Basin (Fig. 1) is a semi-isolated basin situated in the northwestern part of the Weddell Sea. It has an area of approximately $5x10^4$ km^2 and an average water depth of 3,300 km (Coren et al., 1997; Viseras and Maldonado, 1999). The basin, enclosed by the Antarctic Peninsula to the west, the southern Scotia Sea to the north, the South Orkney Microcontinent (SOM) to the east, and the Jane Basin and the Weddell Sea to the South, is at present subject to the clockwise-circulating regime of the Weddell Gyre (Fig. 1). As described in Orsi et al. (1993) and Vernet et al. (2019), the gyre involves four main water masses, namely Antarctic Surface Water (AASW), Warm Deep Water (WDW), Weddell Sea Deep Water (WSDW) and Weddell Sea Bottom Water (WSBW). The AASW generally consists of shelf waters formed over the continental shelves, such as winter water, high salinity shelf water from brine rejection due to sea-ice formation, and ice-shelf water from glacial melt. The shelf waters travel along the Weddell Sea continental shelf via the Antarctic Coastal Current (ACoC) while denser shelf water cascades down and along the continental slope as the Antarctic Slope Current (ASF; Deacon, 1937; Fahrbach et al., 1992; Jacobs, 1991; Thompson et al., 2018). The WDW originates from the warm, saline and low-oxygen Antarctic Circumpolar Current (ACC) that is advected and subsequently integrated into the gyre’s circulation at its eastern front (Orsi et al., 1993; 1995). Along the southern boundary of the Weddell Gyre, the WDW upwells close to the Antarctic margin and mixes with the

https://doi.org/10.5194/egusphere-2024-246
Preprint. Discussion started: 1 February 2024

AASW. The admixture cools and becomes denser, giving rise to the formation of WSDW and WSBW water masses at deeper water depths (Carmack and Foster, 1975; Dorschel, 2019; Huhn et al., 2008). In the Powell Basin, part of the WSDW flows out into the Scotia Sea through channels on the western slope of the basin (namely Philip, Bruce and Discovery Passages; Morozov et al., 2020). The remaining WSDW and a part of WSBW navigate around the southern and eastern South Orkney Plateau, progressing northward via the Orkney Passage as AABW, while the residual WSBW recirculates within the Weddell Gyre (Fedotova and Stepanova, 2021; Gordon et al., 2001; Orsi et al., 1999).

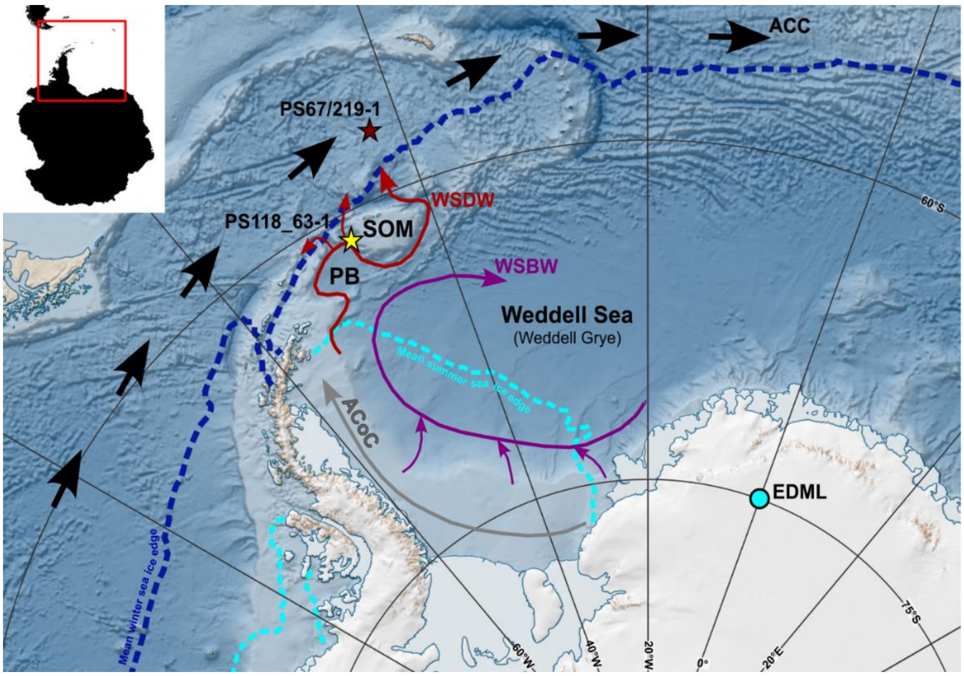

Figure 1. Map of the study area (location with respect to Antarctica indicated by red box in insert map) showing the various oceanographic setting with locations of marine sediment cores PS118_63-1 (yellow star), PS67/219-1 (brown star) and EDML ice core (light blue circle) discussed in this paper. PB: Powell Basin, SOM: South Orkney Microcontinent. Ocean currents and water masses are indicated by solid arrows: Antarctic Circumpolar Current (black), Antarctic Coastal Current (grey), Weddell Sea Deep Water (red) and Weddell Sea Bottom Water (dark magenta). Median winter and summer sea ice extent (1981 – 2010; Fetterer et al., 2017) are illustrated by blue and light blue dotted lines, respectively. Map was adapted from the Norwegian Polar Institute's Qantarctica package using QGIS 3.28 (Matsuoka et al., 2018).

3 Materials and methods

3.1 Sediment core and age model

Gravity core PS118_63-1 was recovered from the Powell Basin during the RV *Polarstern* cruise PS118 to the Weddell Sea in 2019 (Fig. 1; Table 1; Dorschel, 2019). Physical properties, such as magnetic susceptibility (MS) and wet-bulk density, were provided by Frank Niessen (shipboard data; Dorschel, 2019). The age model of core PS118_63-1 is based on ^{14}C radiocarbon dates, the identification of the biostratigraphic marker *Rouxia leventerae*, as well as tuning against records from the EDML ice core ($\delta^{18}O$ and ssNa+) and nearby marine sediment core U1537 (MS, XRF-Fe and opal;

https://doi.org/10.5194/egusphere-2024-246
Preprint. Discussion started: 1 February 2024

Weber et al., 2022). Refer also to Fig. 2 and Supplementary Table S2 for the tie points. Our age model is further substantiated by age constraints of the uranium series disequilibrium, in particular the constant-rate-of-supply model for ^{230}Th-excess (Geibert et al., 2019). Further details on the establishment of the age model and methods are provided in the Supplement S1 and S2.

Table 1. Locations and details of investigated and discussed cores.

Station	Latitude	Longitude	Water depth / Elevation (m)	Recovery (m)	Data source
Marine sediment cores					
PS118_63-1	61° 07.421'S	47° 44.028'W	2626.5	6.88	this study
PS67/219-1	57° 13.22'S	42° 28.02'W	3619	20.71	this study; Xiao et al, 2016a; Xiao et al, 2016b
Ice core					
EDML	75°S	0°	2891		EPICA members, 2006; Fischer et al, 2007

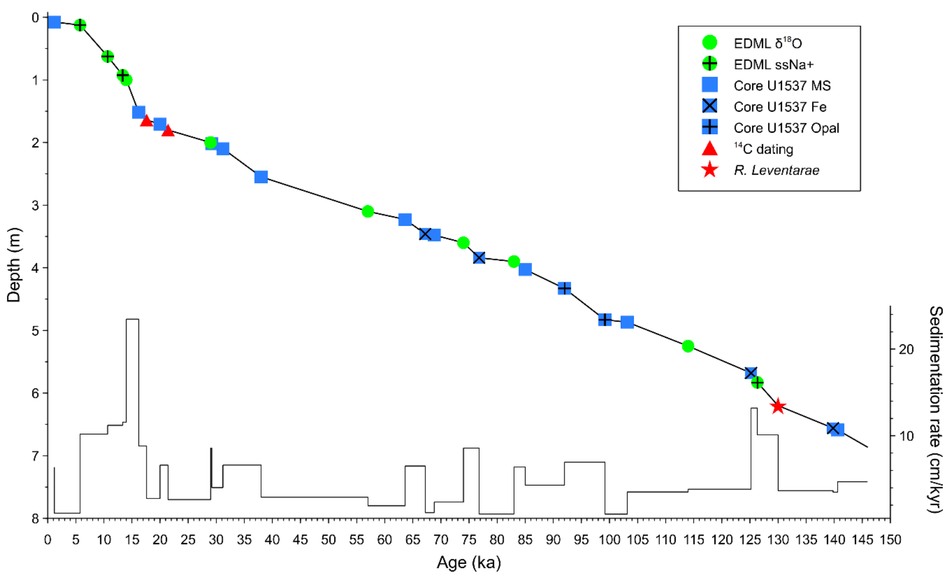

Figure 2.Tie points used for the age-depth model of PS118_63-1. In general, EDML ice core data is indicated by green circles, marine core U1537 data is marked by navy blue square, and available AMS ^{14}C dates and the biostratigraphic marker (R. leventarae) from core PS118_63-1 are depicted by red triangles (^{14}C dates) and a red star (*R. leventarae*).

3.2 Bulk and organic geochemical analyses

A total of 108 sediment samples, each with an approximate thickness of 1 cm, were collected from core PS118_63-1. These samples were then freeze-dried and homogenized using an agate mortar and pestle. All samples were stored in glass vials at -20 °C to prevent degradation. To analyze total organic carbon (TOC), about 0.1 g of sediment was treated with 500 μL of hydrochloric acid to remove any inorganic carbon, including total inorganic carbon and carbonates. After the treatment, the TOC content

https://doi.org/10.5194/egusphere-2024-246
Preprint. Discussion started: 1 February 2024

was measured using a carbon-sulfur determinator (CS800; ELTRA). Biogenic opal was determined using the wet-chemical leaching method following Müller and Schneider (1993).

For biomarker analyses, around 5 – 8 g of sediment was extracted and purified in accordance with well-established protocols (Belt et al., 2012; Lamping et al., 2021). Prior to extraction, internal standards, 7-hexylnonadecane (7-HND) and C_{46}-GDGT, were added for subsequent quantification of HBIs and glycerol dialkyl glycerol tetraether (GDGT) lipids. The biomarkers were extracted via ultrasonication (3 x 15 min) using DCM:MeOH (3 x 10 mL; 2:1 *v*/*v*) as solvent. Thereafter, the extracts were fractionated via open-column chromatography, with SiO_2 as the stationary phase, with the HBI-containing fractions eluted with 5 mL *n*-hexane and the GDGT fractions with 5 mL DCM:MeOH (1:1 *v*/*v*).

Compound analyses of HBIs were performed using an Agilent 7890B Gas Chromatograph (GC; fitted with a 30 m DB 1MS column; 0.25 mm diameter and 0.250 µm film thickness) coupled to an Agilent 5977B Mass Selective Detector (MSD; with 70 eV constant ionization potential, ion source temperature of 230°C). The GC oven temperature was first set to 60°C (3 min), then to 150°C (heating rate of 15°C/min), and finally to 320°C (heating rate of 10°C/min), at which it was held for 15 min for the analysis. Helium was used as the carrier gas. Specific compound identification was based on their retention times and mass spectra characteristics (Belt, 2018; Belt et al., 2000).

Quantification of each biomarker was based on setting the manually integrated GC-MS peak area relative to corresponding internal standards and instrumental-compound response factors. The concentrations were subsequently corrected to the extracted sediment weight. For HBI quantification, the molecular ions *m/z* 348 ($IPSO_{25}$) and m/z 346 (z-/e-trienes) were used in relation to its internal standard 7-HND (*m/z* 266). Finally, all biomarker mass concentrations were normalized to the TOC content of each sample. For calculating $PIPSO_{25}$, we adopted the equation as described in Vorrath et al. (2019):

$$PIPSO_{25} = IPSO_{25} / (IPSO_{25} + (\text{phytoplankton marker} \times c)), \quad (1)$$

where c is the ratio between the mean concentrations of $IPSO_{25}$ and phytoplankton marker and balances any significant offsets between both biomarker concentrations (Müller et al., 2011).

The GDGT fraction was dried (N_2) and redissolved in 120 µL hexane-isopropanol alcohol (99:1 *v*/*v*), followed by filtration through a polytetrafluoroethylene (PTFE) filter with 0.45 µm pore size membrane. GDGT measurement was performed using an Agilent 1200 series high-performance liquid chromatograph coupled to an Agilent 6120 atmospheric pressure chemical ionization mass spectrometer. Identification of isoprenoid GDGTs (isoGDGTs) and branched GDGTs (brGDGTs) was based on retention times and mass-to-charge ratios (isoGDGTs: *m/z* 1302, 1300, 1298, 1296 and 1292; brGDGTs: *m/z* 1050, 1036 and 1022). The late eluting hydroxylated-GDGTs (OH-GDGTs) with molecular ions *m/z* 1318, 1316 and 1314 were also determined during the scan of related isoGDGTs, namely *m/z* 1300, 1298 and 1296, respectively (Liu et al., 2012a; 2012b). The relative abundances were subsequently quantified relative to internal standard C_{46} (*m/z* 744), instrumental response factors and the amount of sediment extracted. Mass content of all GDGTs were normalized to the TOC content of each sample.

https://doi.org/10.5194/egusphere-2024-246
Preprint. Discussion started: 1 February 2024

The calculation of the isoGDGT-based index (Eq 2) and the conversion to subsurface ocean temperature (OT; 0 - 200 m water depth; Eq 3) were calculated in accordance to Kim et al. (2010) and Hagemann et al. (2023):

$$\mathrm{TEX}^{\mathrm{L}}_{86} = \mathrm{Log}_{10} \frac{[\mathrm{isoGDGT{-}2}]}{[\mathrm{isoGDGT{-}1}]+[\mathrm{isoGDGT{-}2}]+[\mathrm{isoGDGT{-}3}]} \quad (2)$$

$$\mathrm{OT}\ (°\mathrm{C}) = 14.38 \times \mathrm{TEX}^{\mathrm{L}}_{86} + 8.93 \quad (3)$$

OH-GDGT-based index (Eq 4) and OT estimation (Eq 5) were determined following Lü et al. (2015):

$$\text{RI-OH'} = \frac{[\mathrm{OH{-}GDGT{-}1}]+2 \times [\mathrm{OH{-}GDGT{-}2}]}{[\mathrm{OH{-}GDGT{-}0}]+[\mathrm{OH{-}GDGT{-}1}]+[\mathrm{OH{-}GDGT{-}2}]} \quad (4)$$

$$\text{RI-OH'} = 0.0382 \times \mathrm{OT}\ (°\mathrm{C}) + 0.1 \quad (5)$$

The index of relative contribution of terrestrial organic matter against that of marine input (branched-isoprenoid tetraether, BIT; Eq 6) was calculated based on Hopmans et al. (2004):

$$\mathrm{BIT} = \frac{[\mathrm{brGDGT{-}I}]+[\mathrm{brGDGT{-}II}]+[\mathrm{brGDGT{-}III}]}{[\mathrm{Crenarchaeol}]+[\mathrm{brGDGT{-}I}]+[\mathrm{brGDGT{-}II}]+[\mathrm{brGDGT{-}III}]} \quad (6)$$

Lastly, we utilize the ring index (RI; Eqs 7 - 9; Zhang et al., 2016) and methanogenic source indicator index (%GDGT-0; Eq 10; Inglis et al., 2015) to validate against possible non-thermal GDGT sources contribution:

$$\mathrm{RI}_{\mathrm{sample}} = 0\mathrm{x}[\mathrm{isoGDGT{-}0}] + 1\mathrm{x}[\mathrm{isoGDGT{-}1}] + 2\mathrm{x}[\mathrm{isoGDGT{-}2}] + 3\mathrm{x}[\mathrm{isoGDGT{-}3}] + 4\mathrm{x}[\mathrm{crenarchaeol}] + 4\mathrm{x}[\text{regio. crenarchaeol'}] \quad (7)$$

$$\mathrm{RI}_{\mathrm{calculated}} = -0.77 \times \mathrm{TEX}_{86} + 3.32 \times (\mathrm{TEX}_{86})^2 + 1.59 \quad (8)$$

$$|\Delta \mathrm{RI}| = \mathrm{RI}_{\mathrm{calculated}} - \mathrm{RI}_{\mathrm{sample}} \quad (9)$$

$$\%\mathrm{GDGT{-}0} = \frac{[\mathrm{GDGT{-}0}]}{[\mathrm{GDGT{-}0}]+[\mathrm{Crenarchaeol}]} \times 100\% \quad (10)$$

3.3 Diatom analyses

41 smear slides were prepared for a quantitative diatom assemblage analysis at respective depths of the core. Between 400 – 600 diatom valves were counted in each sample to ensure statistical significance of the results. Diatoms were identified to species or species group level and, if possible, to forma or variety level. Presence of sea-ice cover is inferred from the percentage of sea-ice indicating diatoms. A combined relative abundance of *Fragilariopsis curta* and *Fragilariopsis cylindus* (hereon referred to as *F. cugr*) of >3% is used as a qualitative threshold to represent presence of WSI, while values between 1 and 3% estimates the edge of maximum winter sea ice (Gersonde et al., 2003; 2005).

https://doi.org/10.5194/egusphere-2024-246
Preprint. Discussion started: 1 February 2024

Likewise, *Fragilariopsis obliquecostata* is used to indicate summer sea ice (SSI) cover (Gersonde and Zielinski, 2000).

We reconstructed WSI concentration (WSIC) by applying a marine diatom transfer function developed by Esper and Gersonde (2014a; TF MAT-D274/28/4an). This transfer function consists of 274 reference samples from surface sediments in the Atlantic, Pacific and western Indian sectors of the SO, with 28 diatom taxa and taxa groups, and an average of 4 analogs (Esper and Gersonde, 2014a). The WSI estimates refer to September SIC averaged over a period between 1981 and 2010 at each surface sediment site (National Oceanic and Atmospheric Adminstration, NOAA; Reynolds et al., 2002; 2007). The reference dataset fits our approach as it uses a 1° by 1° grid, providing a higher resolution than previously used, and giving a root mean square error of prediction of 5.52% (Esper and Gersonde, 2014a).

The SSST were estimated using TF IKM-D336/29/3q, comprising 336 reference samples from surface sediments in the Atlantic, Pacific and western Indian sectors of the SO, with 29 diatom taxa and taxa groups, and a 3-factor model calculated with quadratic regression (Esper and Gersonde, 2014b). The SSST estimates refer to summer (January – March) temperatures at 10 m water depth averaged over a time period from ≤1900 to 1991 (Hydrographic Atlas of the Southern Ocean, HASO; Olbers et al., 1992). The HASO was used because it represents an oceanographic reference dataset least influenced by the recent warming in the SO (Esper and Gersonde, 2014b).

3.4 Comparison with other records

The EDML ice core and the marine sediment core PS67/219-1 are used in this study for regional comparison due to proximity of both cores to our marine core site (Fig. 1; see also Table 1 for details). Water isotope ($\delta^{18}O$) and sea-salt ($ssNa^+$) records of the EDML ice core were investigated by EPICA Members (2006) and Fischer et al. (2007a), respectively. The data is available on Pangaea (EPICA Members, 2010; Fischer et al., 2007b). Marine sediment core PS67/219-1, retrieved from the southern Scotia Sea, is located south of the Polar Front and just north of the modern-day winter sea-ice extent. This core offers data on sea ice, sea surface temperature (SST) and biogenic opal, which extend at least to the LIG period, making it suitable for comparison with inferences from core site PS118_63-1. The chronology and biogenic opal data of core PS67/219-1 was described and published in Xiao et al. (2016b), while investigations on SST and sea-ice reconstruction for the last 30 ka BP are presented in Xiao et al. (2016a). We further review the WSIC using the Imbrie and Kipp Method from Esper and Gersonde (2014a; IKM-D172/28/3q) to achieve a best-fit WSIC estimation for the last 150 kyrs.

3.5 Numerical model

Here, we also analyze model-simulated sea ice, SST and OT estimates for further comparison and evaluation against our proxy results. The model data is derived from climate simulations performed with the Community Earth System Models (COSMOS; Jungclaus et al., 2006). For information on its application, refer to S3.1 in the Supplement. Its atmospheric module is the fifth generation of the European Centre for Medium-Range Weather Forecasts' Model (ECHAM5), a model of the general circulation of the atmosphere with a spectral dynamical core developed at the Max Planck Institute for

https://doi.org/10.5194/egusphere-2024-246
Preprint. Discussion started: 1 February 2024

Meteorology in Hamburg (Stevens et al., 2013). In our model setup, the ECHAM5 is employed at a truncation of T31, corresponding to a spatial resolution of approximately 3.75°x3.75°, or 375 km at the equator. The atmospheric column is discretized at a resolution of 19 vertical hybrid sigma-pressure levels. The ECHAM5 also encompasses a land surface component (JSBACH) that represents multiple land cover classification types (Loveland et al., 2000; Raddatz et al., 2007). We employ JSBACH's capability to reflect vegetation dynamics (Brovkin et al., 2009) in the course climate simulations. In our setup, we consider eight different plant functional types that the model adapts in response to changes in the simulated climate, thereby reflecting important feedback processes between vegetation and climate in our simulations. The ocean module is the Max Planck Institute Ocean Model (MPIOM; Marsland et al., 2003), employed at 40 unevenly spaced pressure levels with a bipolar curvilinear GR30 grid that has a formal resolution of 1.8°x3.0°. This enables the horizontal resolution to reach grid cell dimensions that are as small as 29 km at high latitudes. Sea ice computation is based on dynamic-thermodynamic processes with viscous-plastic rheology and follows the formulation by Hibler (1979). Various parameterizations improve the representation of small-scale ocean dynamics in the simulations. For additional information about the parameterizations utilized in our model setup and the steps taken to create geographic setups to apply the model in paleoclimatological research, see, for example, Stepanek et al. (2020) and references therein.

3.6 Climate simulation

The simulation ensemble consists of a pre-industrial reference state (simulation *piControl*, 1850 CE; Wei and Lohmann, 2012), a Holocene climate (simulation *mh6k*, 6 ka BP; Wei and Lohmann, 2012), an LGM state (simulation *lgm21k*, 21 ka BP; Zhang et al., 2013), two time-slices of the LIG, one for conditions at 125 ka BP (simulation *lig125k*) and one for conditions at 128 ka (simulation *lig128k*), and a Penultimate Glacial Maximum (PGM) climate (simulation *pgm140k*). In order to filter out short-term climate variability on interannual and multidecadal time scales, and to derive average climatic conditions that are representative of the respective Quaternary time-slice, we average the modelled climate state over a period of 100 model years. Further details on the climate states and simulation configurations, refer to S3.2 and Supplementary Table S3, respectively in the Supplement. For analysis purposes, the climate model output is interpolated from the native grid of the ocean model to a regular resolution of 0.25°x0.25°, in order to preserve the geographic features of the ocean model. Additionally, we also derived climate model data specifically tailored to the two marine core sites discussed in this paper, achieving this through interpolating relevant climate fields to the geographic coordinates of each core using a nearest-neighbor interpolation algorithm. Any reference to the modeled sea-ice edges in this publication specifies the isoline of 15% of sea-ice cover.

4 Results

4.1 TOC and Biogenic opal

In this study, both TOC and biogenic opal (Fig. 3) are used as indicators of primary productivity (r = 0.65). The TOC content varies between 0.2 and 0.7% while biogenic opal ranges from 2 to 51%.

https://doi.org/10.5194/egusphere-2024-246
Preprint. Discussion started: 1 February 2024

Highest productivity is observed during MIS 1 and 5e, indicative of favorably warm conditions that promote primary productivity blooms at the core location. A rather moderate productivity level is observed between MIS 5a to c, while lowest values are noted for MIS 2 – 4, 5d and 6. Both profiles also exhibit some differences. For example, peak biogenic opal occurs around 124 ka BP whilst peak TOC is recorded at 119 ka BP. We also observe a more pronounced increase in the TOC content during the terminations than in the biogenic opal content. This is likely due to greater inputs from non-siliceous organisms, such as archaeal, bacterial and terrestrial input (see Supplementary Fig. S4).

4.2 HBIs

The concentration of the sea-ice biomarker ($IPSO_{25}$; Fig. 3) varies significantly between 0 and 2.41 µg/g OC. Peak concentration is found at ca. 112 ka BP, while very low concentrations are noted throughout MIS 2 – 4, 5d, 5e and 6. Moderate to low concentrations are observed during MIS 1 and through both terminations. The concentration of the ice marginal-open water phytoplankton biomarkers varies between 0 - 3.03 µg/g OC (z-triene) and 0 - 0.76 µg/g OC (e-triene; Fig. 3). Higher concentrations are observed at MIS 1 and 5e, while lower concentrations are noted throughout MIS 2 – 4, 5d and 6. In our investigation, we utilized both z- and e-trienes, respectively, to calculate the semi-quantitative spring/summer sea-ice indices ($P_{z/e}IPSO_{25}$). This combined use of biomarkers, indicative of ice marginal-open water conditions and $IPSO_{25}$, helps to circumvent ambiguous interpretations especially when dealing with scenarios of permanent sea-ice cover and open ocean conditions. Our P_zIPSO_{25} index ranges between 0.09 and 1, while the P_eIPSO_{25} index varies from 0.06 to 1. Instances, where both values of $IPSO_{25}$ and z-/e-triene are zero, the $P_{z/e}IPSO_{25}$ index is assigned a value of 1, indicating permanent ice cover. Both index profiles presented a similar trend ($r = 0.98$), with higher values (> 0.8) throughout MIS 2 – 4, 5d and 6, while reduced values noted for MIS 1 and 5e. Notably, the lowest $P_{z/e}IPSO_{25}$ values (< 0.2) are observed during MIS 5e, specifically between 119 and 128 ka BP, signifying a distinct decline in sea ice and more open ocean condition during this time interval. Comparable low $P_{z/e}IPSO_{25}$ values are also observed around 4 and 12 ka BP.

https://doi.org/10.5194/egusphere-2024-246
Preprint. Discussion started: 1 February 2024

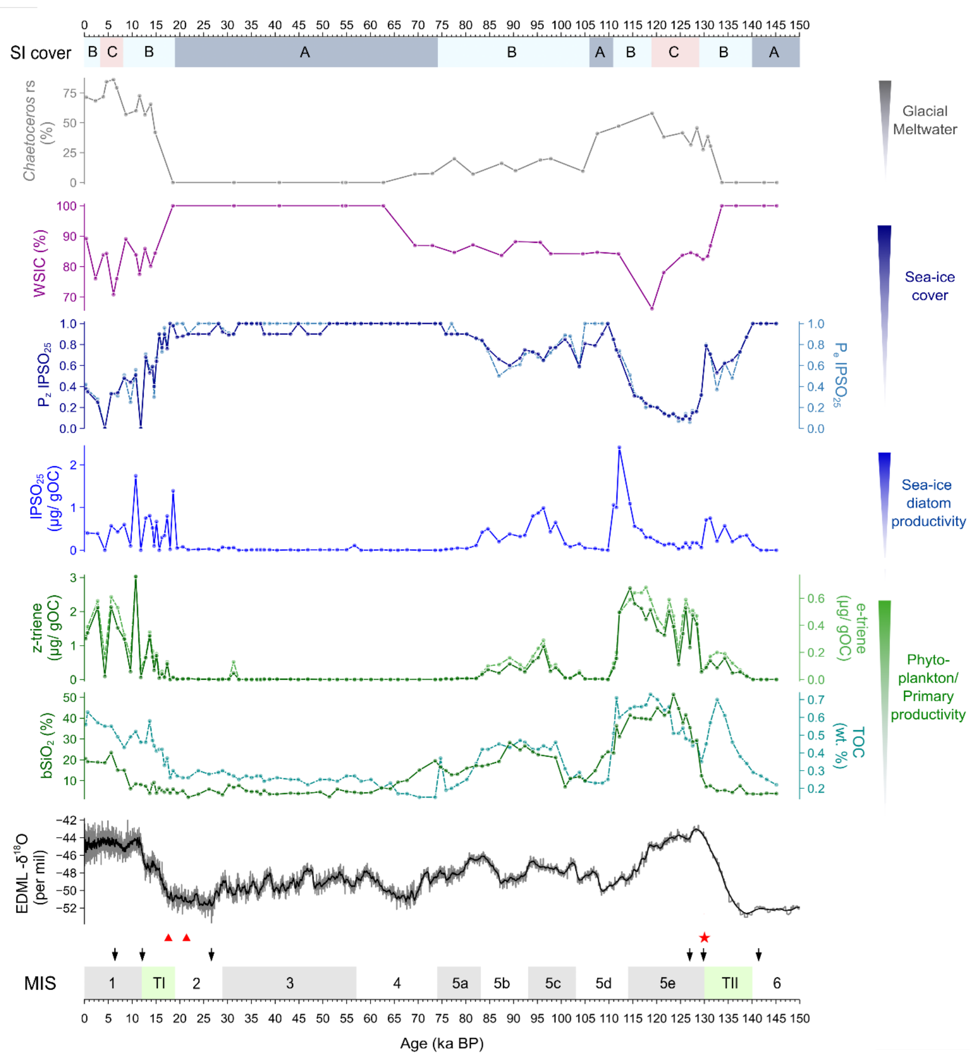

Figure 3. Multiproxy analyses of sea ice conditions in Powell Basin, reconstructed from marine sediment core PS118_63-1. Sea-ice (SI) cover scenarios: A - permanent sea-ice cover (dark blue), B - dynamic sea-ice cover (light blue) and C - minimal sea-ice cover (light red). Glacial meltwater indicator: Chaetoceros resting spores, Sea ice indicators: Diatom-based winter sea-ice concentration (WSIC), HBI-based Phytoplankton-IPSO$_{25}$ index (PIPSO$_{25}$) and IPSO$_{25}$. Productivity indicators: HBI z-/e-trienes, biogenic opal (bSiO$_2$), and total organic carbon (TOC). Atmospheric temperature is implied by the δ^{18}O record from the EDML ice core. AMS ^{14}C dates are marked with red triangles, the biostratigraphic marker (R. leventarae) is indicated by the red star. The black arrows delineated the time-slices for the model simulations in this study. MIS stages are depicted in alternating grey (odd) and white (even) shades, while the terminations TI and TII are shown in green.

4.3 GDGTs

Downcore OT estimates using the RI-OH' index cover a temperature range between -2.5 and 1.0°C (Fig. 4) while TEX$_{86}^{L}$-derived OT fluctuates between -2.6 and 1.0°C (Supplementary Fig. S5). Certainly, these minimum temperatures of less than -1.9°C – freezing temperature of seawater – need to be considered with caution as the calibration equations for RI-OH' and TEX$_{86}^{L}$ are based on datasets

https://doi.org/10.5194/egusphere-2024-246
Preprint. Discussion started: 1 February 2024

with residual errors of 6°C (Lü et al., 2015) and 0.6°C (Hagemann et al., 2023), respectively. Other factors influencing the ocean temperature calibration include bias from terrestrial input, water depth, use of satellite-assigned ocean temperature below the freezing point of seawater and inadequate samples from polar areas (Fietz et al., 2020; Xiao et al., 2023). Nevertheless, both OT proxies consistently indicate a cold-water subsurface regime (0 – 200 m; < 1°C) with a 0 – 2°C temperature fluctuation, and no significant glacial/interglacial variability, over the last 145 kyrs. Calculation of GDGT-related indices such as BIT, %GDGT-0 and ΔRI (Supplementary Fig. S5) reveals the presence of potential non-thermal influences on the TEX_{86}^{L} index, which may lead to bias in the temperature reconstruction (see also S4 in the Supplement). In light of the conflicting trends and potential non-thermal influences, we have decided not to further discuss on the TEX_{86}^{L}-derived OT in this paper.

4.4 Diatoms

The diatom-based data for cores PS118_63-1 and PS67/219-1 are presented in Fig. 4. For core PS118_63-1 from the Powell Basin, the relative abundance of sea ice-related diatoms ranges between 2 and 39% for *F. cugr*, and from 0 to 6% for *F. obliquecostata*. The relative abundance of diatoms between ca. 15 and 70 ka BP, and before 131 ka BP, is rare/absent (Fig. 4). Such cases generally indicate the presence of permanent sea-ice cover over the core site (Zielinski and Gersonde, 1997). We, therefore, assign the diatoms' relative abundance as 0, and WSIC as 100%, to above-mentioned time intervals (i.e., MIS 2 - 4 and 6). The abundance of *F. cugr* is noted to be above the 3% threshold (indicative of presence of WSI) throughout the remaining time periods – except at 6 ka BP, where the lowest abundance (2%) is registered. Whereas, the relative abundance of *F. obliquecostata* fluctuates around the 3% threshold, likely indicating a dynamic summer sea-ice edge over the area during MIS 1 and 5. The WSIC across the rest of the time frame, namely MIS 1 and 5, are generally high (>75%) as well, with a couple of lower WSIC observed at ca. 6 ka BP (71%) and at 119 ka BP (66%). The abundance of *Chaetoceros* resting spores (*Chaetoceros* rs) varies between 0 and 86%, with higher values noted during MIS 1 and 5e (Fig. 3). Such increases in the abundance of the *Chaetoceros* rs imply presence of glacial meltwater at the core location (Crosta et al., 1997). The diatom-derived SSST record with a range between -0.8 and 0.4°C describes a cold-water region during MIS 1 and 5, similar to the RI-OH'-derived OT.

To the north in the southern Scotia Sea, core PS67/219-1 documents an overall lower percentage of sea ice-related diatoms. Similar to core PS118_63-1, the relative abundance of *F. cugr* (0.5 – 20%) is noted to be mostly above the 3% threshold, indicating presence of WSI over the region, with higher abundance observed for MIS 2 and 3, and lowest abundance (<1%) observed during MIS 5e. However, the relative abundance of *F. obliquecostata* for core PS67/219-1 remains below the 3% threshold, between 0 and 3%, suggesting a lack of SSI cover over the core site. The percentage of WSIC in the southern Scotia Sea is also lower than at Powell Basin, having a record of 37 – 82%, with the lowest WSIC noted at MIS 5e. The diatom-based SSST documents a SSST range of -0.7 to 2°C, with colder SSST registered during MIS 2 and 3, and warmer SSST noted during MIS 1 and 5e.

https://doi.org/10.5194/egusphere-2024-246
Preprint. Discussion started: 1 February 2024

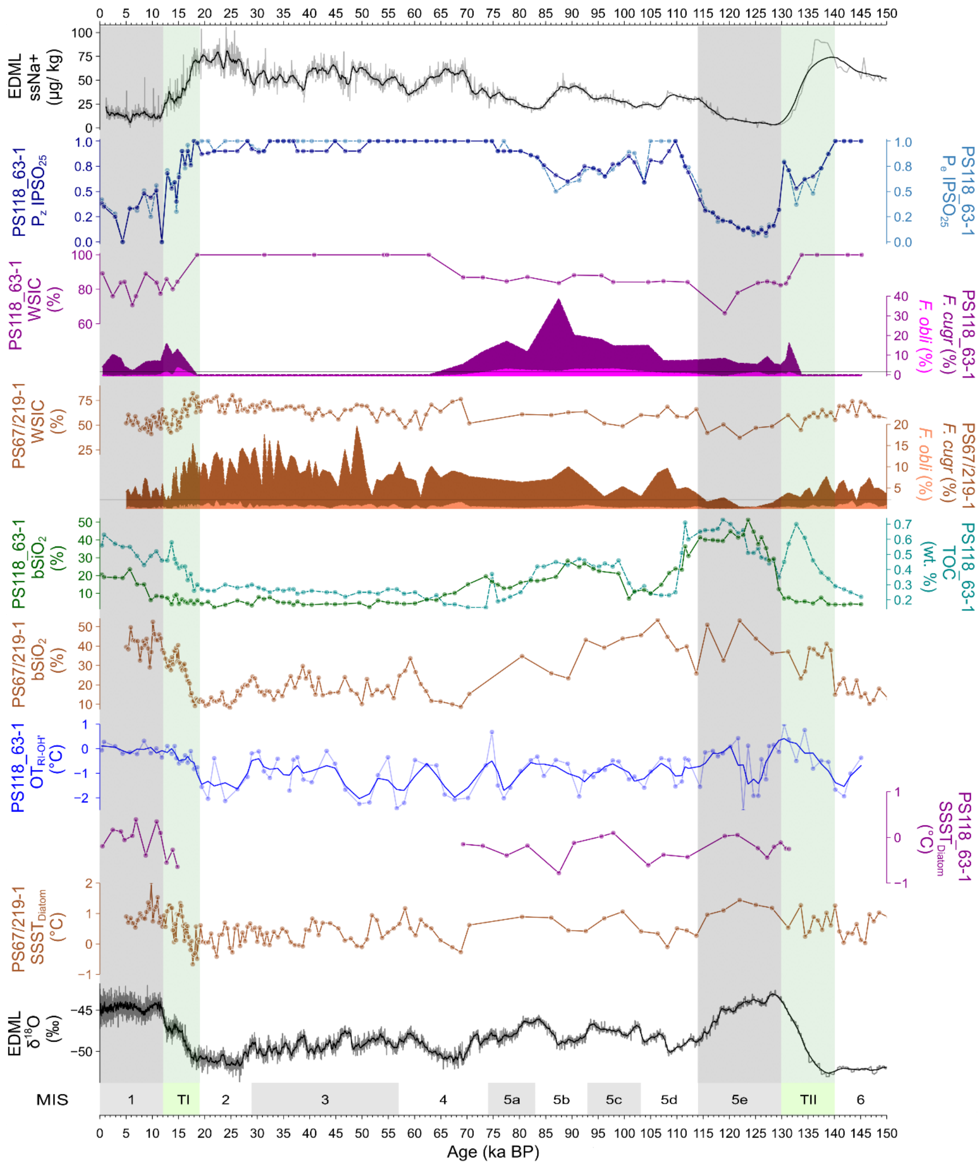

Figure 4. Regional sea ice, productivity and temperature variability in the South Atlantic sector of the Southern Ocean. Particularly, Powell Basin (PS118_63-1): diatom-based winter sea ice concentration (WSIC - dark magenta), F. curta group (F. cugr - dark magenta), F. obliquecostata (F. obli - light magenta), HBI-based sea ice indicator (P_zIPSO_{25} - dark blue; P_eIPSO_{25} - dotted light blue), productivity indicators ($bSiO_2$ – dark green; TOC – dotted light green), RI-OH'-derived subsurface ocean temperature ($OT_{RI-OH'}$ – navy blue) and summer sea surface temperature ($SSST_{Diatom}$ – dark magenta). Southern Scotia Sea (PS67/219-1): diatom-based WSIC (brown), F. curta group (F. cugr - brown), F. obliquecostata (F. obli - light brown), productivity ($bSiO_2$ – brown) and $SSST_{Diatom}$ (brown). While the EDML ice core provides reference temperature and sea ice concentration for the region. The 3% threshold for diatom species relative abundance is indicated by a black horizontal line. MIS stages are depicted in alternating grey (odd) and white (even) shades, while the terminations TI and TII are shown in green.

https://doi.org/10.5194/egusphere-2024-246
Preprint. Discussion started: 1 February 2024

4.5 Sea ice conditions – a multiproxy approach

Using a multiproxy approach, our analysis of the data from core PS118_63-1 provides a continuous glacial-interglacial sea ice history in the Powell Basin since the PGM. We distinguish three different sea-ice scenarios, spanning the last 145 kyrs (Fig. 3).

A) Perennial sea-ice cover. This scenario is characterized by remarkably low (sea-ice) diatom abundances, minimum $IPSO_{25}$ and HBI-triene concentrations, as well as minimum $bSiO_2$ and TOC contents. We deduce the presence of maximum WSIC and a spring/summer sea-ice ($PIPSO_{25}$) cover. These results indicate a glacial setting, with our core site situated under a perennial sea-ice or ice-shelf cover and exposed to minimal primary production in the water column. Such a scenario persisted throughout the glacial periods MIS 2 – 4, MIS 6, and during MIS stadial 5d.

B) Dynamic sea-ice cover. This scenario is described by fluctuations in each of the proxy profiles, in particular WSIC, $PIPSO_{25}$, HBI-trienes, $bSiO_2$ and TOC contents. These records reflect the dynamic nature of sea-ice conditions over our core site, with varied primary production at different time intervals. This scenario is prevalent during periods of climate transition, such as terminations I and II, and during MIS 1 and 5a-c.

C) Minimal (winter-only) sea-ice cover. This scenario is denoted by a considerably reduced sea-ice diatom ($IPSO_{25}$) production, WSIC and $PIPSO_{25}$, coupled with high phytoplankton productivity (HBI-trienes), $bSiO_2$ and TOC contents. These findings suggest that our core site experienced ice-free or winter-only ice conditions, permitting enhanced primary production in the water column. This scenario occurs in short time intervals within the interglacials, for example, 8 – 5 ka BP (MIS 1) and 130 – 119 ka BP (MIS 5e).

4.6 Inferences from numerical climate simulations

Here, we present our model-simulated sea ice, SST and OT (220 m water depth), covering the Atlantic sector of the SO, at six glacial-interglacial time-slices: PGM at 140 ka BP, LIG at 128 (sea ice only) and 125 ka BP, LGM at 21 ka BP, Holocene at 6 ka BP and pre-industrial (Fig. 5 - 7). For Fig. 5, the left column (Fig. 5a) shows the simulated sea-ice estimation/extent for the spring/summer seasons (NDJFMA, this averaging period considers the time lag in sea-ice extent vs. spring/summer temperature evolution) while the right column (Fig. 5b) illustrates the simulated sea-ice estimation/extent for the winter (ASO) season. In general, a greater sea-ice estimation is generally observed during winter than spring/summer for each time-slice. During the glacial periods, the model highlights a northward expansion of the sea-ice extent beyond both marine core sites (PGM: Fig. 5.1; LGM: Fig. 5.4). At the more southern site (Powell Basin; core PS118_63-1), the modeled glacial sea-ice estimation varies between ~93 to 94% (winter) and ~79 to 82% (spring/summer), while at the more northern site (southern Scotia Sea; core PS67/219-1), sea-ice estimation varies around ~91% (winter) and ~26 to 34% (spring/summer). In contrast, during the interglacials, the sea-ice extent fluctuates between seasons. WSI extent is observed to be located north of both core sites (Fig. 5.2b, 5.3b, 5.5b and 5.6b), with the WSI estimation ranging between ~86 and 89% at core site PS118_63-1, and ~52 to 69% at core site PS67/219-1. While during spring/summer, the sea-ice extent retreats to a latitude between both sites

https://doi.org/10.5194/egusphere-2024-246
Preprint. Discussion started: 1 February 2024

(Fig. 5.2a, 5.3a, 5.5a and 5.6a), with the spring/summer sea-ice estimation varying from ~31 to 35% at core site PS118_63-1 and between ~0 and 4% at core site PS67/219-1.

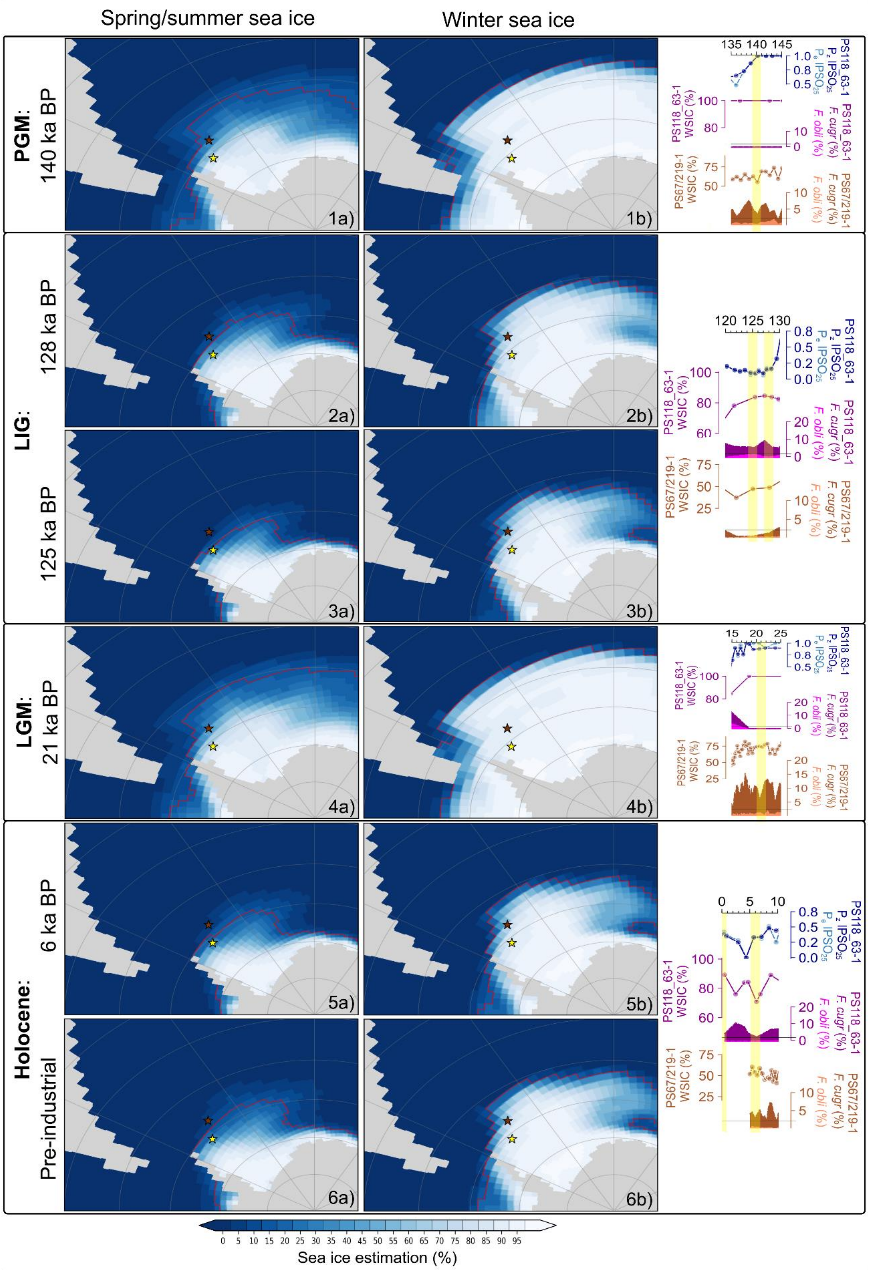

Figure 5. Model-simulated mean a) spring/summer (NDJFMA) and b) winter (ASO) sea ice estimation for the various time slices: 1) PGM: 140 ka BP, 2) LIG: 128 ka BP, 3) LIG: 125 ka BP, 4) LGM: 21 ka BP, 5) mid-Holocene: 6 ka BP and 6) Pre-industrial. The red line depicts the sea ice extent and is defined as the isoline of 15% sea ice coverage. Location of marine sediment cores is indicated with stars: PS118_63-1 (yellow) and PS67/219-1 (brown). Proxy-derived winter sea ice concentration (WSIC), sea ice-related diatom abundance and spring/summer sea ice cover (PIPSO$_{25}$) for each time slice are in yellow shadings.

https://doi.org/10.5194/egusphere-2024-246
Preprint. Discussion started: 1 February 2024

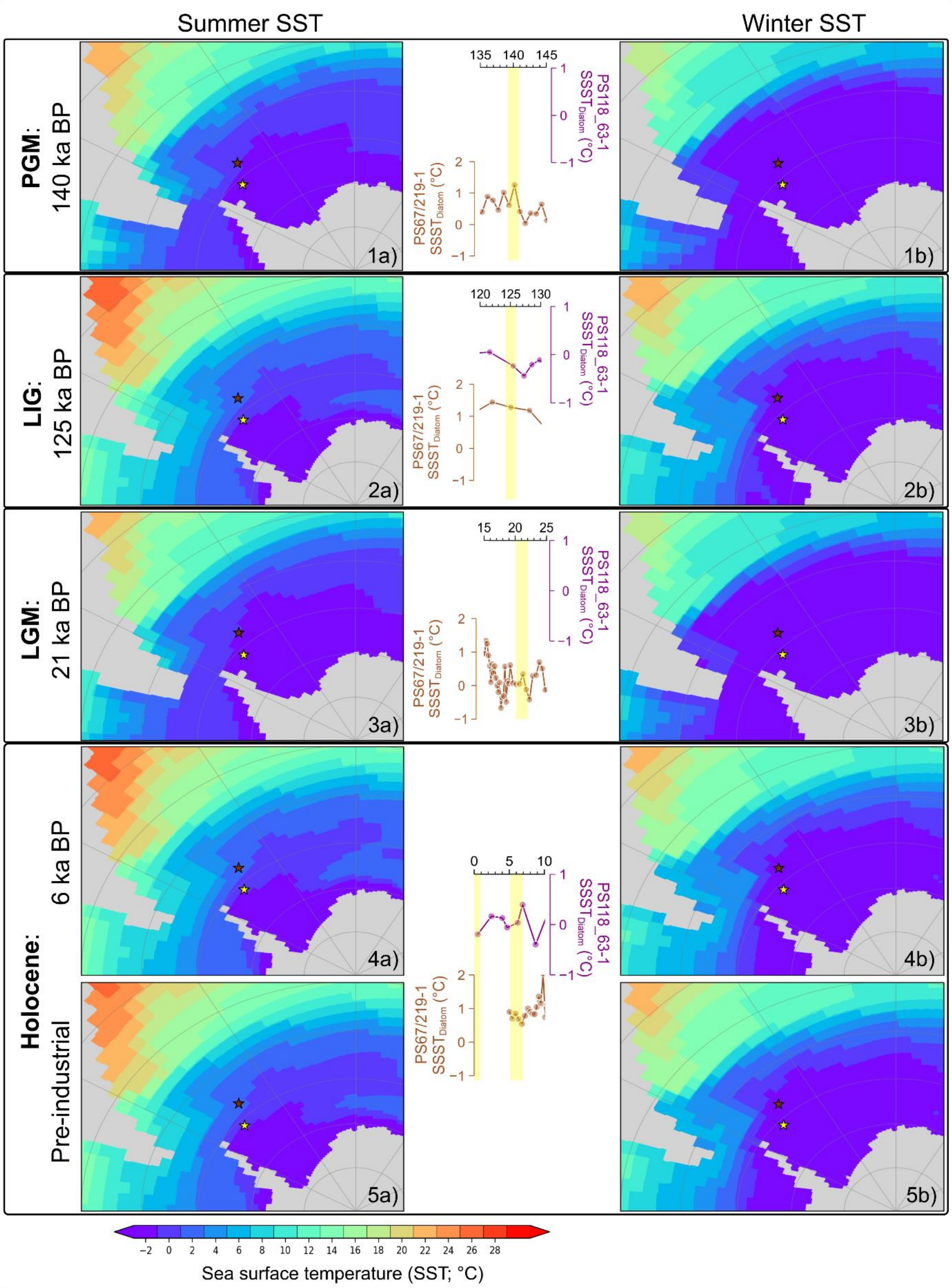

Figure 6. Model-simulated mean a) summer (DJF) and b) winter (JJA) sea surface temperature (SST) for the various time slices: 1) PGM: 140 ka BP, 2) LIG: 125 ka BP, 3) LGM: 21 ka BP, 4) mid-Holocene: 6 ka BP and 5) Pre-industrial. Marine sediment cores, PS118_63-1 (yellow) and PS67/219-1(brown), are indicated by the coloured stars. Diatom-based summer sea surface temperature ($SSST_{Diatom}$) for the respective time slice is highlighted in yellow.

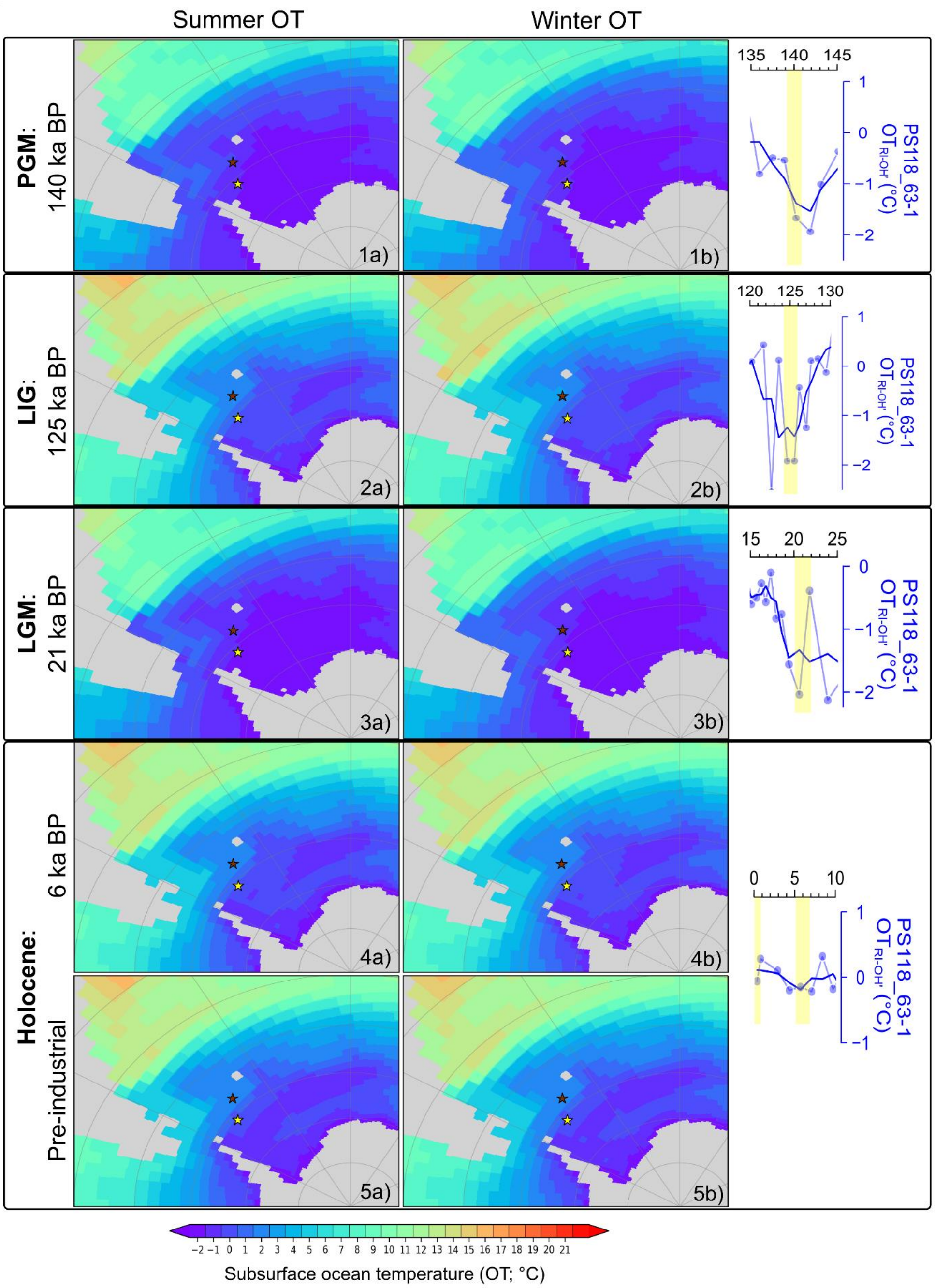

Figure 7. Model-simulated mean a) summer (DJF) and b) winter (JJA) subsurface ocean temperature (OT) for the various time slices: 1) PGM: 140 ka BP, 2) LIG: 125 ka BP, 3) LGM: 21 ka BP, 4) mid-Holocene: 6 ka BP and 5) Pre-industrial. Marine sediment cores are presented in coloured stars: PS118_63-1 (yellow) and PS67/219-1(brown). Biomarker-based ocean temperature ($OT_{RI-OH'}$) for the respective time slice is indicated by the yellow shadings

For the SST and OT, the left columns (Fig. 6a and 7a) represent the summer (DJF) temperature, and the right columns (Fig. 6b and 7b) depicts the winter (JJA) temperatures, respectively. The simulated result observed for the SST (Fig. 6) appears similar to that of the modelled sea ice output. In general, widespread, low SST, close to the freezing point of seawater (that is approximately -1.9°C at salinity values modelled in the SO in our simulations), is exhibited across all time-slices during winter (Fig. 6b), while in summer (Fig. 6a), low SST mainly occurs in the Weddell Sea and along the coast of the Antarctic continent. For instance, at the core site PS118_63-1 in Powell Basin, Weddell Sea, there is no observed difference in SST between winter and summer during the glacial periods PGM (Fig. 6.1) and LGM (6.3). Both sites were surrounded by sea ice during these periods (Fig. 5.1 and 5.4). However, in interglacials, a seasonal SST cycle of ~1°C is noted in the basin (Fig. 6.2, 6.4 and 6.5). In contrast, at the more northern core site PS67/219-1, the model estimates a seasonal SST cycle of ~1°C during the glacial periods (Fig. 6.1 and 6.3) and ~3.4°C during the interglacial (Fig. 6.2, 6.4 and 6.5). Moreover, the modeled climate states are characterized by spatial SST gradients between the two core locations of between 0°C (glacial) and ~0.4°C (interglacial) during winter. For summer SST, the gradient between the two core locations varies between ~1°C (glacial) and ~2.8°C (interglacial). As for the simulated OT, the model simulates a ~1.6 and ~3°C glacial-interglacial variation at core sites PS 118_63-1 and PS67/219-1, respectively, but no appreciable OT change is observed between seasons if the glacial-interglacial variability range is taken as a reference (Fig. 7). The model also reveals a spatial OT gradient between both marine core sites of ~0.7°C (glacial) and ~2.1°C (interglacial).

5 Discussion

5.1 Regional sea-ice and oceanic conditions

5.1.1 Penultimate Glacial Maximum – Termination II

Our records showed that during the PGM, the Powell Basin (core PS118_63-1) remained under a layer of persistent (sea) ice cover, as evidenced by a 100% WSIC and peak $PIPSO_{25}$ values. This coincided with the lowest levels of primary productions observed in the biogenic opal and TOC records. This condition persisted until ca. 140 ka BP, when a decline in spring/summer sea ice ($PIPSO_{25}$) is observed, accompanied by a rise in TOC and subsurface ocean temperature (Fig. 4). While at a more northernly location in the southern Scotia Sea, core PS67/219-1 records a more dynamic sea ice condition during PGM. High WSIC (fluctuating at around 65%), together with a 1 – 3% abundance of *F. obliquecostata,* suggest the proximity of a permanent sea-ice edge. These findings from the geological record are supported by our model simulation for the 140 ka BP time-slice, which shows an overall high WSI estimation (94%; 92%), but slightly lower spring/summer sea-ice estimation (79%; 27%) at core sites PS118_63-1 and PS67/219-1, respectively (Fig. 5a). Likewise, higher $ssNa^+$ concentrations and $\delta^{18}O$ values from EDML ice core point to cold conditions and an extensive sea ice cover in the Atlantic region (EPICA Community Members, 2006; Fischer et al., 2007a).

Termination II (TII; 140 – 130 ka BP) marks the transition from a glacial into an interglacial environment. The onset of this deglaciation was probably initiated by a warming event caused by maximum southern high latitude summer insolation at around 138 ka BP (Bianchi and Gersonde, 2002;

Broecker and Henderson, 1998) and further sustained by the Heinrich Stadial 11 (HS11) event occurring in the Northern Hemisphere (NH) between 135 and 130 ka BP (Turney et al., 2020). The HS11 is a prominent North Atlantic meltwater event that may have triggered the eventual shutdown of the AMOC, thus reinforcing the warming in the SO via the bipolar seesaw effect (Marino et al., 2015).

In the Powell Basin, the WSIC remains high (100%) and only starts to decrease (80%) at ca. 134 ka BP, while gradually declining $PIPSO_{25}$ values since 140 ka BP accompany the onset of the deglaciation and mark a shift from perennial sea ice to dynamic seasonal sea-ice cover (see Sect 4.5 for a definition). A concurrent rise in subsurface ocean temperature is also observed during this timeframe. In contrast, core PS67/219-1 in the southern Scotia Sea recorded a different sea-ice regime. An oscillating decline in WSIC and <1% abundance of *F. obliquecostata* suggest a variable WSI cover with a distal summer sea-ice edge. The different sea-ice conditions in both regions are supported by a higher biogenic opal production recorded in the southern Scotia Sea as compared to the minimum biogenic opal content observed for the Powell Basin (Fig. 4). The Powell Basin TOC profile is also different from its opal counterpart, with the former peaking between 135 – 131 ka BP. We surmise that this peak may relate to a preferential growth environment for non-siliceous marine organisms and/or increased input of terrestrial organic matter during this interval.

The persistent warming was interrupted by a short period of spring/summer sea ice ($PIPSO_{25}$) re-expansion and weakened decline in WSI towards the end of TII (ca. 132 – 130 ka BP), along with an increasing *Chaetoceros RS* abundance that peaks at ca. 131 ka BP (Fig. 4). These conditions coincide with the northward shift of the sea-ice edge at ODP Site 1094 around 129.5 ka BP (Bianchi and Gersonde, 2002). A comparable reduction in SSST at around 131 ka BP is also observed in the southern Scotia Sea (core PS67/219-1, Fig. 4) and apparent at ODP Site 1089 and core PS2821-1 (Cortese and Abelmann, 2002). In the Powell Basin, this cooling event is also associated with reduced primary production, although no decline in temperature is detected (Fig. 4). Considering age uncertainties, we postulate that the sea-ice expansion and ocean cooling are part of the same event, likely influenced by meltwater influx as a result of cavern(s) expansion beneath major Antarctic ice shelves (such as the Filchner-Ronne Ice Shelf; Ashley et al., 2021; Hellmer, 2004).

5.1.2 Last Interglacial - MIS 5 stadials/interstadials

Following the short-lived sea-ice expansion in Powell Basin at the end of TII, we observe a rapid decline, and minimum spring/summer sea-ice cover is reached (see Sect 4.5) by ca. 129 ka BP (Fig. 4). Lowest spring/summer sea ice ($PIPSO_{25}$) is observed between 126 and 124 ka BP, while minimum WSIC is observed around 119 ka BP. These conditions promoted primary productivity, as reflected in the maximum biogenic opal and TOC contents, at the respective timeframes (Fig. 4). Likewise, sea ice and temperature profiles from core PS67/219-1, the EDML ice core and model simulations also favor a warm and predominately open ocean condition for the South Atlantic sector throughout the LIG (Fig. 4, 5.3 and 6.3; EPICA Community Members, 2006; Fischer et al., 2007a). Holloway et al. (2017) investigated the simulated-spatial structure of the Antarctic WSI minimum at 128 ka BP with respect to the $\delta^{18}O$-isotopic peak recorded in the East Antarctica ice cores. They tested numerous WSI retreat scenarios and concluded that the $\delta^{18}O$ maximum could be explained by a significant decline in Antarctic

https://doi.org/10.5194/egusphere-2024-246
Preprint. Discussion started: 1 February 2024

WSI, with the Atlantic sector experiencing the largest reduction of 67%. Contrastingly, while our spring/summer sea-ice ($PIPSO_{25}$) data aligns with their $\delta^{18}O$-accorded simulated-findings, our diatom data - revealing a constant presence of WSI in the Powell Basin with even minor increases between 130 and 127 ka BP - disagrees. Our interpretation is, that such inconsistency could possibly be linked to sea-ice variations between seasons (Bova et al., 2021; Renssen et al., 2005). Moreover, our simulated sea-ice estimation at the 128 ka BP time-slice corroborates our proxy-based data, indicating the presence of WSI in the region amidst lower sea-ice concentration and continued retreat of sea ice over the spring/summer seasons (Fig. 5.2). A similar sea-ice scenario is also established for the 125 ka BP time-slice, known to be the warmest period of the LIG (Fig. 5.3; Goelzer et al., 2016; Hoffman et al., 2017), where Southern Hemisphere (SH) mid- to high-latitude spring insolation forcing reached a maximum within the period from 130 ka BP to 125 ka BP (Lunt et al., 2013). The contrasting observation between our marine sediment proxy and model data against that of the ice core $\delta^{18}O$-accorded simulated-finding emphasizes the need for more robust marine-based reconstructions, especially south of the modern sea-ice edge, to sufficiently substantiate model results for these regions, and to enable comprehensive input knowledge for future model simulations and predictions (Holloway et al., 2017; Otto-Bliesner et al., 2013).

The reconstructed SSST trends in the Powell Basin and the southern Scotia Sea are largely comparable with the atmospheric temperature profile from the EDML ice core, suggesting atmosphere-ocean interactions in the regions. The lack of significant glacial-interglacial temperature variability within the Powell Basin could potentially be linked to its locality and close proximity to the continental margin, where constant mixing of cold ice-shelf water with the warm deep water (WDW) persists. Within the Powell Basin, both the SSST and subsurface ocean temperature started to decrease around 130 ka BP. While the SSST appeared to have cooled from -0.2°C to -0.4°C (127 ka BP) and recovered thereafter – similar to the dip observed in the EDML $\delta^{18}O$ profile, the subsurface ocean temperature declined distinctly from 0 to ca. -1.9°C and remained cold until 124 ka BP (Fig. 4). This approximate 3-kyr interval of further-reduced subsurface temperature coincided with a brief surge in the North Atlantic Deep Water (NADW) formation, instigated by the collapse of the AABW between 127 and 125 ka BP (Hayes et al., 2014). This event triggered an intense incursion of WDW upon a receding West Antarctic Ice Sheet (WAIS) margin, resulting in the discharge of a substantial volume of meltwater into the southern Weddell Sea (Marino et al., 2015). We hypothesize that, similar to modern-day Weddell Gyre circulation (see Sect 2 for details), this cold ice-shelf meltwater pulse probably made its way into the Powell Basin via the ACoC and ASF and deepened the cold-water stratification in the basin thus causing the short-lived extreme cold subsurface water regime observed between 127 and 124 ka BP. There has been substantial evidence supporting a significant retreat (or collapse) of the WAIS during the LIG (Holloway et al., 2016; Joughin and Alley, 2011; Mercer, 1968; Steig et al., 2015). For example, Turney et al. (2020) discovered that the WAIS had retreated from the Patriot Hills blue ice area by the end of TII (130.1 ± 1.8 ka BP). This area is located 50 km inland from the present-day grounding line of the Filchner-Ronne Ice Shelf. Their investigation revealed a 50 kyrs hiatus in the blue ice record, indicative of a collapse of the ice-shelf at the end of TII, followed by its subsequent recovery during late MIS 5. Holloway et al. (2016) also propose a maximum ice sheet retreat around 126 ka BP based on distinct

https://doi.org/10.5194/egusphere-2024-246
Preprint. Discussion started: 1 February 2024

differences between the isotopic records observed for Mt Moulton and East Antarctic ice cores. Assuming that, the distinct reduction in spring/summer sea ice recorded in core PS118_63-1 was not confined to the Powell Basin but may reflect a more extensive sea ice decline in the Weddell Sea embayment, we posit that this loss of sea ice (i.e. the loss of an effective buffer protecting ice-shelf fronts) may have accelerated the disintegration of the Weddell Sea ice-shelves and, ultimately, the WAIS.

Following the peak of the LIG around 119 ka BP, the Powell Basin sea-ice records reflect a cycle of sea-ice advance and retreat throughout the remaining MIS 5 substages. WSIC strengthened and remained at ca. 80%, while spring/summer sea ice ($PIPSO_{25}$) experienced a substantial increase between MIS 5e and 5d (reaching PGM values at 5d), and remained elevated (> ca. 0.6) for the rest of the MIS. This expansion of sea ice into MIS 5d, and its persisting presence throughout the remaining MIS 5, is accompanied by a gradual decline in both sea surface and subsurface ocean temperatures, along with reduced primary production (Fig. 4). Likewise, an increasing WSIC, lowered SSST and primary productivity are also noted in the southern Scotia Sea. However, being more northernly located, the southern Scotia Sea experienced a lower and more varied WSIC (ca. 48 - 68%), with a distal summer sea-ice edge evident by a lower abundance of *F. obliquecostata* (<1%) than the Powell Basin (Fig. 4).

5.1.3 Glacial period – Last Glacial Maximum – Termination I

After MIS 5, Antarctica transited into the last glacial period (74 – 19 ka BP). In our Powell Basin records, this reflects a northward expansion of the sea-ice extent (peak $PIPSO_{25}$ values and 100% WSIC). Additionally, the lack of sea ice- and phytoplankton-related biomarkers and diatoms points towards an extremely suppressed production in the basin (Fig. 3 and 4). We postulate that at that time the basin was likely covered by permanent sea-ice cover or a floating ice-shelf, which inhibited primary production in the underlying water column. The southern Scotia Sea record (PS67/219-1) further to the north also presents an overall higher winter and summer sea ice cover, with elevated abundance of *F. obliquecostata* (0 - 3%) during this period suggesting a permanent sea-ice edge close to the core site (Xiao et al., 2016a). The oscillating patterns observed in both the sea-ice record and the biogenic opal content further point to alternating advance and retreat phases of the sea-ice edge in the southern Scotia Sea (Allen et al., 2011).

In the Powell Basin, capped by an overlying (sea) ice cover throughout the glacial period, subsurface ocean temperatures somewhat resemble the millennial-scale variability in the EDML temperature profile (Fig. 4). We presume that the subsurface temperature variations may possibly reflect changes in the ocean circulation in the Atlantic sector of the SO (Böhm et al., 2015; Williams et al., 2021). However, the resolution of our subsurface ocean temperature record is too low to make an affirmative conclusion, and more data points will be required to ascertain corresponding oceanic variability.

The last glacial period culminated during the LGM between 26.5 and 19 ka BP with a most northwardly extending sea-ice edge, as identified in several marine sediment cores (Gersonde et al., 2005; Xiao et al., 2016a) and deduced from maximum sea-salt concentrations in the EDML ice core

https://doi.org/10.5194/egusphere-2024-246
Preprint. Discussion started: 1 February 2024

(Fig. 4; Fischer et al., 2007a). Evidence from previous studies indicated the advance of grounded ice sheet and island ice caps to the edge of the outer continental shelf (Davies et al., 2012; Dickens et al., 2014). These grounded ice sheets were surrounded by floating ice-shelves that extended seaward to 58°S on the western side of Antarctica (Herron and Anderson, 1990; Johnson and Andrews, 1986). In the Atlantic sector, the 60 - 70% expansion of WSI towards the modern Polar Front (~50°S; Gersonde et al., 2003) also promoted a northward shift of the SSI edge beyond core site PS67/219-1 to around 55°S (Allen et al., 2011; Collins et al., 2012), which lead to restricted primary productivity as reflected in the minimum biogenic opal content of core PS67/219-1 (Fig. 4). The LGM is also considered the coldest interval, with a northward expansion of the (sub)Antarctic cold waters by 4 - 5° in latitude towards the subtropical warm waters (Gersonde and Zielinski, 2000; Gersonde et al., 2003). Sea-ice extent (Fig. 5.4) and SSST (Fig. 6.3) derived from our climate simulation during the peak of LGM (21 ka BP) align with these findings. This distinct growth of the (sea) ice-field in the Southern Ocean, coupled with lower reconstructed and modelled LGM subsurface temperatures (Fig. 4 and 7.3), suggests an intensified cold-water stratification at our core sites. According to Ferrari et al. (2014), during the LGM, the upwelling zone of the circumpolar deep water shifted further from the continental margin, nearing the edge of the SSI field. In this period, intensified AABW penetrated northward into the deep North Atlantic, causing the NADW to shoal above 2 km water depth (Curry and Oppo, 2005). This displacement of the NADW has a profound impact on heat distribution in deep-ocean circulation, as vertical mixing of the AABW and NADW – typically occurring below 2 km water depth in proximity to seamounts and midocean ridge – is prevented. Consequently, greater volume of cold AABW, rather than warm NADW, was recirculated back to the SO as circumpolar deep water (Ferrari et al., 2014; Watson et al., 2015).

TI began around 18 ka BP, when our records from Powell Basin indicate a transition from a perennial-ice cover to a dynamic sea-ice scenario (see Sect 4.5), with several cycles of advance and retreat. Similarly, the sea ice-related records from the southern Scotia Sea (PS67/219-1) and the EDML sea-salt record depict a decrease in sea-ice cover, along with rapid increases in primary productivity and ocean temperature (Fig. 4). This deglaciation is attributed to a weakening AMOC circulation as a result of reduced NADW formation caused by increasing NH summer insolation and significant ice sheet melt at 18 ka BP, also known as Heinrich Stadial 1 (Clark et al., 2020; Denton et al., 2010; Waelbroeck et al., 2011). The gradual warming of TI was interrupted by a brief cooling between 14 and 12 ka BP. During this interval, our records reveal a short-term re-advancement in sea ice, coupled with a drop in productivity and temperature (Fig. 4). This event seems to coincide with multiple South Atlantic records (Xiao et al., 2016a) and higher sea-salt concentrations and a plateau in $\delta^{18}O$ values recorded in the EDML ice core (Fischer et al., 2007a). We believe this event to be the Antarctic Cold Reversal (ACR), which is linked to the Bølling-Allerød warm interval in the NH via the bipolar seesaw mechanism (Pedro et al., 2011; 2016).

5.1.4 Holocene

Following the brief cooling of the ACR, the deglacial warming resumed its pace and Antarctica transited into the present interglacial (Holocene: 12 ka BP – present), which is marked by intervals of

https://doi.org/10.5194/egusphere-2024-246
Preprint. Discussion started: 1 February 2024

warming and cooling events (Bentley et al., 2009; Bianchi and Gersonde, 2004; Xiao et al., 2016a). Our data support these findings and document periods characterized by seasonal/dynamic and minimum sea-ice cover (see Sect 4.5) since 12 ka BP. We acknowledge that the age constraints of core PS118_63-1 for the Holocene is limited but still permit the discrimination of different warm and cold intervals. The first post-ACR warming is noted between 12 and 9 ka BP, while a possible second warming is observed between 8 and 5 ka BP.

The Powell Basin experienced a rapid decline in the winter and spring/summer sea-ice, concurrent with a rise in SSST (-0.5 to 0.5°C) and primary productivity between 12 and 9 ka PB, suggesting a seasonal sea-ice cover. In contrast, between 8 and 5 ka BP, our proxy data reveals significant reduction in the abundance of *F. cugr* (below 3% threshold), WSIC and spring/summer sea ice ($PIPSO_{25}$). This, alongside a further elevated primary productivity signal, may indicate a brief open-ocean setting for the Powell Basin during this warm interval (Fig. 4). While at the southern Scotia Sea, trace levels (<1%) of *F. obliquecostata* recorded in core PS67/219-1, coupled with a fluctuating WSI cover, centering around 50%, implies an open-ocean condition with occasional WSI in the region. Interestingly, a higher – though varying – SSST (0.6 to 2.0°C) and peak biogenic production is observed between 12 and 9 ka BP, while a less elevated SSST (0.5 to 1°C) and biogenic production is observed between 8 and 5 ka BP (Fig. 4; Xiao et al., 2016a). The cooling and mild warming experienced in the southern Scotia Sea between 9 and 5 ka BP probably indicate a northward export of increased glacial meltwater from the Weddell Sea (Powell Basin) – substantiated by the elevated presence of *Chaetoceros* rs recorded in core PS118_63-1 (Fig. 3). Our model simulation at 6 ka BP depicts a somewhat similar oceanic condition, with <40% spring/summer sea ice at the studied sites. However, in comparison with our proxy records, the model appears to have overestimated the WSI, SST and OT. This overestimation may be attributed to the complex ice-ocean interactions and feedbacks of the Antarctic coastal region, which may not be fully represented in the model that has a spatial resolution in the order of tens of kilometers.

We propose that a distinct Holocene climate optimum occurred at each core site, as evident from our findings. For example, the southern Scotia Sea witnessed the climate optimum from 12 to 9 ka BP (Xiao et al., 2016a), whereas the warmest interval (Holocene) in the Powell Basin occurred between 8 and 5 ka BP. Michalchuk et al. (2009) also established similar deglacial conditions for the northern Antarctic Peninsula – where the ice sheet/glacier retreated by 8.3 ka BP, followed by the mid-Holocene climate optimum between 8.3 and 6 ka BP. Moreover, the climate optimum experienced in the Powell Basin corresponds to the mid-Holocene climate optimum identified in sediment cores from the South Orkney Plateau between 8.2 and 4.8 ka BP and around Antarctica (Crosta et al., 2008; Denis et al., 2010; Kim et al., 2012; Lee et al., 2010; Taylor et al., 2001). However, reports of differing timings and mode for the mid-Holocene climate optimum around Antarctic Peninsula have been noted in previous studies (Bentley et al., 2009; Davies et al., 2012; Shevenell et al., 1996; Taylor and Sjunneskog, 2002). Vorrath et al. (2023) determined the mid-Holocene climate optimum to have occurred between 8.2 and 4.2 ka BP, based on biomarker analyses of a marine core from eastern Bransfield Strait. They suggest that the climatic changes at their core site were influenced predominantly by the warm ACC rather than the cold-water Weddell Sea. This is contrary to a shorter climate optimum (6.8 – 5.9 ka BP) proposed by Heroy et al. (2008), where they examined the climate history of western Bransfield Strait using sediment and diatom analyses. Such diverse research outcomes highlight the complexity of responses to micro-region variations in glacial, atmospheric and oceanic changes in the Antarctic Peninsula throughout the Holocene (Bentley et al., 2009; Davies et al., 2012; Heroy et al., 2008; Vorrath et al., 2023).

5.2 Comparison between interglacials / transition periods

A comparison of the environmental changes caused by climate warming during TII and TI as well as the peak LIG and the Holocene, may yield valuable information on common or different driving and feedback mechanisms. As marine cores PS118_63-1 and PS67/219-1 provide continuous records of the environmental evolution in the northwestern Weddell Sea and southern Scotia Sea, respectively, dating back to at least 145 ka BP, they offer a distinct opportunity to evaluate (sea-ice) conditions between the two terminations (TII and TI) and both warm periods (LIG and Holocene), particularly in proximity to the continental margin. Denton et al. (2010) studied the last four terminations and concluded that the terminations were triggered by a sequence of comparable events: maximum NH summer insolation that caused substantial NH ice sheet melting (due to marine ice sheet instability) over an extended (>5 kyrs) NH stadial interval. The huge release of meltwater slowed the AMOC, thus triggering an intense warming in the southern high-latitudes through the bipolar seesaw teleconnection, accompanied by a poleward shift in the southern westerlies. Our records from cores PS118_63-1 and PS67/219-1 portray a consistent and rapid decline in sea ice throughout both terminations (TII and TI). Interestingly, both deglaciations feature a short-term re-advancement of sea ice during their latest stage, ca. 130 ka BP and the ACR, respectively, likely due to meltwater-discharge from retreating ice-shelves/ice sheets in the Southern Ocean. This suggests that sea-ice growth stimulated by deglacial meltwater may be a common feature during glacial terminations. Despite commonalities in the sea-ice records, some differences are discernible. For instance, an abrupt surge in biogenic opal in the southern Scotia Sea, alongside a continuous rise in TOC content within the Powell Basin, can be observed for TII. In contrast, TI exhibits a saw-toothed pattern for these proxies. Additionally, the southern Scotia Sea recorded a higher mean biogenic opal and SSST across TII (35%; 0.7°C) than TI (26%; 0.5°C). Likewise, in the Powell Basin, higher mean TOC, SSST and subsurface ocean temperature are perceived during TII (0.5%; -0.3°C; -0.03°C) than TI (0.4%; -0.5°C; -0.4°C). These variations likely reflect differing deglacial magnitudes experienced in the South Atlantic across the two terminations. For instance, the EDML $\delta^{18}O$ record registered a stronger deglacial amplitude (32%) in TII than TI (Masson-Delmotte et al., 2011). Broecker and Henderson (1998) also speculated that the amplitude of the SH summer insolation during TII was higher than TI. Additionally, a delay of approximately 10 kyrs between the SH and NH summer insolation (and subsequent NH ice sheet melting) during TII – as compared to TI's SH summer insolation peak just before the melting of the NH ice sheet – probably contributed to a more pronounced TII warming than TI in the Southern Ocean.

The climate during the LIG appeared to be warmer than the Holocene. In the Powell Basin, the LIG peak interval (i.e., MIS 5e) was characterized by a significantly reduced spring/summer sea-ice cover and peak productivity, while a higher spring/summer sea-ice cover, along with an only gradually increasing productivity are observed for the Holocene warm period (Fig. 4). Bova et al. (2021)

https://doi.org/10.5194/egusphere-2024-246
Preprint. Discussion started: 1 February 2024

hypothesized that the LIG was relatively warmer than the Holocene as a result of its preceding deglacial dynamics: specifically, the magnitude of the last deglaciation was half that of the penultimate deglaciation – where a rapid and intense warming destabilized and significantly reduced the (sea) ice cover to near modern-day level by the onset of the LIG (Bova et al., 2021) and possibly a collapse of the WAIS in the first half of the LIG (Pollard and Deconto, 2009; Sutter et al., 2016). As such, we opine that the lower magnitude warming during TI resulted in a spatially and temporally varying retreat and advance of (sea) ice cover (including ice-shelves and glaciers) in the Southern Ocean. This is witnessed in our rather variable Holocene sea-ice proxy records (Fig. 4) and differing reports of mid-Holocene warming and repeated fluctuations in environmental conditions around the Antarctica (see sect 5.1.4; Bentley et al., 2014; Davies et al., 2012; Ó Cofaigh et al., 2014).

6 Summary and conclusions

Multiproxy analyses on marine sediment core PS118_63-1 from the Powell Basin provide new insights into the glacial-interglacial environmental variability in proximity to the Antarctic continental margin. With the use of the novel sea-ice and open-water biomarkers and diatom assemblage data, alongside primary productivity proxies, we are able to reconstruct sea-ice conditions in the Powell Basin for the past ca. 145 kyrs. Our findings reveal year-round ice-cover with minimal productivity during glacial periods, while dynamic sea-ice conditions with varied productivity are recorded in the Powell Basin during climate transitions and interglacial periods, such as the Holocene and MIS 5. Peak reduction in sea ice and near open ocean conditions are noted for MIS 5e. In contrast, no significant glacial-interglacial temperature variation was registered in the basin, which is in line with the generally cold-water regime of Weddell Sea. Comparison between the current and last interglacial, and their corresponding climate transitions (TI and TII) suggests a relationship between deglacial amplitude and warming intensity during the corresponding interglacial: in general, an abrupt and intense (gradual and slow) deglaciation leads to a warmer (cooler) interglacial, with higher (lesser) ice sheet retreat (Bova et al., 2021). Our data presented in this study reinforce earlier paleo sea-ice reconstructions in the South Atlantic sector of the SO and provide fresh insights into the ice-proximal sea-ice response during varying climate conditions. Evaluation of both proxy and model data highlights similarities between sea-ice reconstruction and simulation. However, notable discrepancies are observed for the Holocene and subsurface temperature estimations. It is therefore pivotal to expand on these paleoclimate data, to further close the gap in our understanding of ocean-ice-atmosphere interactions and dynamics towards enhancing climate model predictions closer to the Antarctic continental margins.

Data availability. Data mentioned in this article will be available on the PANGAEA - Data Publisher for Earth & Environmental Science. (address; citation)

Supplement. The supplement related to this article is available online at:

Author contributions. This study was conceived by WWK and JM. Data collection and interpretation was conducted by WWK, together with OE (diatom), JM (HBI), JH and GM (GDGT). WG produced the U/Th-dating data. CS and GL selected, documented, and postprocessed the data from an ensemble of simulations that provided the climate model data for this study. Three of the six simulations presented here, namely lig125k, lig128k, and pgm140k, represent previously unpublished climate model output created by PG. WX supplied unpublished data for PS67/219-1. WWK wrote the paper and created the visualizations, supported by CS who visualized model output and interpolated climate model output to core locations. JM supervised the study. All authors contributed to the analyses, discussion of the results, and the conclusion of this study.

Competing interests. The authors declare that they have no conflict of interest.

Acknowledgements. We thank the captain, crew and science team of the RV Polarstern cruise PS118 (Grant No. AWI_PS118_04). Special appreciation is also extended to Denise Diekstall (HBI), Mandy Kuck (HBI), Ulrike Böttjer (Biogenic Opal) for their support. Simon Belt is acknowledged for providing the 7-HND internal standard for HBI quantification. This research is funded through the Alfred Wegener Institute Helmholtz Centre for Polar and Marine Research (International Science Program for Integrative Research in Earth Systems, INSPIRES II).

References

Abernathey, R. P., Cerovecki, I., Holland, P. R., Newsom, E., Mazloff, M., and Talley, L. D.: Water-mass transformation by sea ice in the upper branch of the Southern Ocean overturning, Nature Geoscience, 9, 596-601, 10.1038/ngeo2749, 2016.

Allen, C. S., Pike, J., and Pudsey, C. J.: Last glacial–interglacial sea-ice cover in the SW Atlantic and its potential role in global deglaciation, Quaternary Science Reviews, 30, 2446-2458, https://doi.org/10.1016/j.quascirev.2011.04.002, 2011.

Ashley, K. E., McKay, R., Etourneau, J., Jimenez-Espejo, F. J., Condron, A., Albot, A., Crosta, X., Riesselman, C., Seki, O., Massé, G., Golledge, N. R., Gasson, E., Lowry, D. P., Barrand, N. E., Johnson, K., Bertler, N., Escutia, C., Dunbar, R., and Bendle, J. A.: Mid-Holocene Antarctic sea-ice increase driven by marine ice sheet retreat, Clim. Past, 17, 1-19, 10.5194/cp-17-1-2021, 2021.

Barbara, L., Crosta, X., Schmidt, S., and Massé, G.: Diatoms and biomarkers evidence for major changes in sea ice conditions prior the instrumental period in Antarctic Peninsula, Quaternary Science Reviews, 79, 99-110, https://doi.org/10.1016/j.quascirev.2013.07.021, 2013.

Barbara, L., Crosta, X., Leventer, A., Schmidt, S., Etourneau, J., Domack, E., and Massé, G.: Environmental responses of the Northeast Antarctic Peninsula to the Holocene climate variability, Paleoceanography, 31, 131-147, https://doi.org/10.1002/2015PA002785, 2016.

Belt, S. T.: Source-specific biomarkers as proxies for Arctic and Antarctic sea ice, Organic Geochemistry, 125, 277-298, https://doi.org/10.1016/j.orggeochem.2018.10.002, 2018.

Belt, S. T. and Müller, J.: The Arctic sea ice biomarker IP25: a review of current understanding, recommendations for future research and applications in palaeo sea ice reconstructions, Quaternary Science Reviews, 79, 9-25, https://doi.org/10.1016/j.quascirev.2012.12.001, 2013.

Belt, S. T., Allard, W. G., Massé, G., Robert, J.-M., and Rowland, S. J.: Highly branched isoprenoids (HBIs): identification of the most common and abundant sedimentary isomers, Geochimica et Cosmochimica Acta, 64, 3839-3851, https://doi.org/10.1016/S0016-7037(00)00464-6, 2000.

Belt, S. T., Brown, T. A., Rodriguez, A. N., Sanz, P. C., Tonkin, A., and Ingle, R.: A reproducible method for the extraction, identification and quantification of the Arctic sea ice proxy IP25 from marine sediments, Analytical Methods, 4, 705-713, 10.1039/C2AY05728J, 2012.

Belt, S. T., Smik, L., Brown, T. A., Kim, J. H., Rowland, S. J., Allen, C. S., Gal, J. K., Shin, K. H., Lee, J. I., and Taylor, K. W. R.: Source identification and distribution reveals the potential of the geochemical Antarctic sea ice proxy IPSO25, Nature Communications, 7, 12655, 10.1038/ncomms12655, 2016.

Bentley, M. J., Hodgson, D. A., Smith, J. A., Cofaigh, C. Ó., Domack, E. W., Larter, R. D., Roberts, S. J., Brachfeld, S., Leventer, A., Hjort, C., Hillenbrand, C.-D., and Evans, J.: Mechanisms of Holocene palaeoenvironmental change in the Antarctic Peninsula region, The Holocene, 19, 51-69, 10.1177/0959683608096603, 2009.

Bentley, M. J., Ó Cofaigh, C., Anderson, J. B., Conway, H., Davies, B., Graham, A. G. C., Hillenbrand, C.-D., Hodgson, D. A., Jamieson, S. S. R., Larter, R. D., Mackintosh, A., Smith, J. A., Verleyen, E., Ackert, R. P., Bart, P. J., Berg, S., Brunstein, D., Canals, M., Colhoun, E. A., Crosta, X., Dickens, W. A., Domack, E., Dowdeswell, J. A., Dunbar, R., Ehrmann, W., Evans, J., Favier, V., Fink, D., Fogwill, C. J., Glasser, N. F., Gohl, K., Golledge, N. R., Goodwin, I., Gore, D. B., Greenwood, S. L., Hall, B. L., Hall, K., Hedding, D. W., Hein, A. S., Hocking, E. P., Jakobsson, M., Johnson, J. S., Jomelli, V., Jones, R. S., Klages, J. P., Kristoffersen, Y., Kuhn, G., Leventer, A., Licht, K., Lilly, K., Lindow, J., Livingstone, S. J., Massé, G., McGlone, M. S., McKay, R. M., Melles, M., Miura, H., Mulvaney, R., Nel, W., Nitsche, F. O., O'Brien, P. E., Post, A. L., Roberts, S. J., Saunders, K. M., Selkirk, P. M., Simms, A. R., Spiegel, C., Stolldorf, T. D., Sugden, D. E., van der Putten, N., van Ommen, T., Verfaillie, D., Vyverman, W., Wagner, B., White, D. A., Witus, A. E., and Zwartz, D.: A community-based geological reconstruction of Antarctic Ice Sheet deglaciation since the Last Glacial Maximum, Quaternary Science Reviews, 100, 1-9, https://doi.org/10.1016/j.quascirev.2014.06.025, 2014.

Bianchi, C. and Gersonde, R.: The Southern Ocean surface between Marine Isotope Stages 6 and 5d: Shape and timing of climate changes, Palaeogeography, Palaeoclimatology, Palaeoecology, 187, 151-177, https://doi.org/10.1016/S0031-0182(02)00516-3, 2002.

Bianchi, C. and Gersonde, R.: Climate evolution at the last deglaciation: the role of the Southern Ocean, Earth and Planetary Science Letters, 228, 407-424, https://doi.org/10.1016/j.epsl.2004.10.003, 2004.

Böhm, E., Lippold, J., Gutjahr, M., Frank, M., Blaser, P., Antz, B., Fohlmeister, J., Frank, N., Andersen, M. B., and Deininger, M.: Strong and deep Atlantic meridional overturning circulation during the last glacial cycle, Nature, 517, 73-76, 10.1038/nature14059, 2015.

Bova, S., Rosenthal, Y., Liu, Z., Godad, S. P., and Yan, M.: Seasonal origin of the thermal maxima at the Holocene and the last interglacial, Nature, 589, 548-553, 10.1038/s41586-020-03155-x, 2021.

Broecker, W. S. and Henderson, G. M.: The sequence of events surrounding Termination II and their implications for the cause of glacial-interglacial CO2 changes, Paleoceanography, 13, 352-364, https://doi.org/10.1029/98PA00920, 1998.

Brovkin, V., Raddatz, T., Reick, C. H., Claussen, M., and Gayler, V.: Global biogeophysical interactions between forest and climate, Geophysical Research Letters, 36, https://doi.org/10.1029/2009GL037543, 2009.

Carmack, E. C. and Foster, T. D.: On the flow of water out of the Weddell Sea, Deep Sea Research and Oceanographic Abstracts, 22, 711-724, https://doi.org/10.1016/0011-7471(75)90077-7, 1975.

Chadwick, M., Allen, C. S., Sime, L. C., and Hillenbrand, C. D.: Analysing the timing of peak warming and minimum winter sea-ice extent in the Southern Ocean during MIS 5e, Quaternary Science Reviews, 229, 106134, https://doi.org/10.1016/j.quascirev.2019.106134, 2020.

Chadwick, M., Allen, C. S., Sime, L. C., Crosta, X., and Hillenbrand, C. D.: Reconstructing Antarctic winter sea-ice extent during Marine Isotope Stage 5e, Clim. Past, 18, 129-146, 10.5194/cp-18-129-2022, 2022.

Chadwick, M., Jones, J., Lawler, K.-A., Prebble, J., Kohfeld, K. E., and Crosta, X.: Understanding glacial-interglacial changes in Southern Ocean sea ice, Past Global Changes Magazine, 27(2), 86, https://doi.org/10.22498/pages.27.2.86, 2019.

Clark, P. U., He, F., Golledge, N. R., Mitrovica, J. X., Dutton, A., Hoffman, J. S., and Dendy, S.: Oceanic forcing of penultimate deglacial and last interglacial sea-level rise, Nature, 577, 660-664, 10.1038/s41586-020-1931-7, 2020.

Collins, L. G., Pike, J., Allen, C. S., and Hodgson, D. A.: High-resolution reconstruction of southwest Atlantic sea-ice and its role in the carbon cycle during marine isotope stages 3 and 2, Paleoceanography, 27, https://doi.org/10.1029/2011PA002264, 2012.

Collins, L. G., Allen, C. S., Pike, J., Hodgson, D. A., Weckström, K., and Massé, G.: Evaluating highly branched isoprenoid (HBI) biomarkers as a novel Antarctic sea-ice proxy in deep ocean glacial age sediments, Quaternary Science Reviews, 79, 87-98, https://doi.org/10.1016/j.quascirev.2013.02.004, 2013.

COREN, F., CECCONE, G., LODOLO, E., ZANOLLA, C., ZITELLINI, N., BONAZZI, C., and CENTONZE, J.: Morphology, seismic structure and tectonic development of the Powell Basin, Antarctica, Journal of the Geological Society, 154, 849-862, 10.1144/gsjgs.154.5.0849, 1997.

Cortese, G. and Abelmann, A.: Radiolarian-based paleotemperatures during the last 160 kyr at ODP Site 1089 (Southern Ocean, Atlantic Sector), Palaeogeography, Palaeoclimatology, Palaeoecology, 182, 259-286, https://doi.org/10.1016/S0031-0182(01)00499-0, 2002.

Crosta, X., Denis, D., and Ther, O.: Sea ice seasonality during the Holocene, Adélie Land, East Antarctica, Marine Micropaleontology, 66, 222-232, https://doi.org/10.1016/j.marmicro.2007.10.001, 2008.

Crosta, X., Pichon, J.-J., and Labracherie, M.: Distribution of Chaetoceros resting spores in modern peri-Antarctic sediments, Marine Micropaleontology, 29, 283-299, https://doi.org/10.1016/S0377-8398(96)00033-3, 1997.

Crosta, X., Kohfeld, K. E., Bostock, H. C., Chadwick, M., Du Vivier, A., Esper, O., Etourneau, J., Jones, J., Leventer, A., Müller, J., Rhodes, R. H., Allen, C. S., Ghadi, P., Lamping, N., Lange, C. B., Lawler, K. A., Lund, D., Marzocchi, A., Meissner, K. J., Menviel, L., Nair, A., Patterson, M., Pike, J., Prebble, J. G., Riesselman, C., Sadatzki, H., Sime, L. C., Shukla, S. K., Thöle, L., Vorrath, M. E., Xiao, W., and Yang, J.: Antarctic sea ice over the past 130,000 years – Part 1: a review of what proxy records tell us, Clim. Past, 18, 1729-1756, 10.5194/cp-18-1729-2022, 2022.

Curry, W. B. and Oppo, D. W.: Glacial water mass geometry and the distribution of δ13C of ΣCO2 in the western Atlantic Ocean, Paleoceanography, 20, https://doi.org/10.1029/2004PA001021, 2005.

Davies, B. J., Hambrey, M. J., Smellie, J. L., Carrivick, J. L., and Glasser, N. F.: Antarctic Peninsula Ice Sheet evolution during the Cenozoic Era, Quaternary Science Reviews, 31, 30-66, https://doi.org/10.1016/j.quascirev.2011.10.012, 2012.

Deacon, G.: The hydrography of the southern ocean, Discovery Rep, 15, 1-124, 1937.

DeConto, R. M. and Pollard, D.: Contribution of Antarctica to past and future sea-level rise, Nature, 531, 591-597, 10.1038/nature17145, 2016.

Denis, D., Crosta, X., Barbara, L., Massé, G., Renssen, H., Ther, O., and Giraudeau, J.: Sea ice and wind variability during the Holocene in East Antarctica: insight on middle–high latitude coupling, Quaternary Science Reviews, 29, 3709-3719, https://doi.org/10.1016/j.quascirev.2010.08.007, 2010.

https://doi.org/10.5194/egusphere-2024-246
Preprint. Discussion started: 1 February 2024

Denton, G. H., Anderson, R. F., Toggweiler, J. R., Edwards, R. L., Schaefer, J. M., and Putnam, A. E.: The Last Glacial Termination, Science, 328, 1652-1656, doi:10.1126/science.1184119, 2010.

Dickens, W. A., Graham, A. G. C., Smith, J. A., Dowdeswell, J. A., Larter, R. D., Hillenbrand, C.-D., Trathan, P. N., Erik Arndt, J., and Kuhn, G.: A new bathymetric compilation for the South Orkney Islands region, Antarctic Peninsula (49°–39°W to 64°–59°S): Insights into the glacial development of the continental shelf, Geochemistry, Geophysics, Geosystems, 15, 2494-2514, https://doi.org/10.1002/2014GC005323, 2014.

Dieckmann, G. S. and Hellmer, H. H.: The importance of sea ice: an overview, in: Sea ice, edited by: Dieckmann, G. S., and Hellmer, H. H., Blackwell Science Ltd, 1-22, 2010.

Dorschel, B.: The Expedition PS118 of the Research Vessel POLARSTERN to the Weddell Sea in 2019, Alfred Wegener Institute for Polar and Marine Research, Bremerhaven, 10.2312/BzPM_0735_2019, 2019.

Ebert, E. E., Schramm, J. L., and Curry, J. A.: Disposition of solar radiation in sea ice and the upper ocean, Journal of Geophysical Research: Oceans, 100, 15965-15975, https://doi.org/10.1029/95JC01672, 1995.

Esper, O. and Gersonde, R.: New tools for the reconstruction of Pleistocene Antarctic sea ice, Palaeogeography, Palaeoclimatology, Palaeoecology, 399, 260-283, https://doi.org/10.1016/j.palaeo.2014.01.019, 2014a.

Esper, O. and Gersonde, R.: Quaternary surface water temperature estimations: New diatom transfer functions for the Southern Ocean, Palaeogeography, Palaeoclimatology, Palaeoecology, 414, 1-19, https://doi.org/10.1016/j.palaeo.2014.08.008, 2014b.

Etourneau, J., Collins, L. G., Willmott, V., Kim, J. H., Barbara, L., Leventer, A., Schouten, S., Sinninghe Damsté, J. S., Bianchini, A., Klein, V., Crosta, X., and Massé, G.: Holocene climate variations in the western Antarctic Peninsula: evidence for sea ice extent predominantly controlled by changes in insolation and ENSO variability, Clim. Past, 9, 1431-1446, 10.5194/cp-9-1431-2013, 2013.

Fahrbach, E., Rohardt, G., and Krause, G.: The Antarctic coastal current in the southeastern Weddell Sea, Polar Biology, 12, 171-182, 1992.

Fedotova, A. A. and Stepanova, S. V.: Water Mass Transformation in the Powell Basin, in: Antarctic Peninsula Region of the Southern Ocean: Oceanography and Ecology, edited by: Morozov, E. G., Flint, M. V., and Spiridonov, V. A., Springer International Publishing, Cham, 115-129, 10.1007/978-3-030-78927-5_8, 2021.

Ferrari, R., Jansen, M. F., Adkins, J. F., Burke, A., Stewart, A. L., and Thompson, A. F.: Antarctic sea ice control on ocean circulation in present and glacial climates, Proceedings of the National Academy of Sciences, 111, 8753-8758, doi:10.1073/pnas.1323922111, 2014.

Fietz, S., Ho, S. L., and Huguet, C.: Archaeal Membrane Lipid-Based Paleothermometry for Applications in Polar Oceans, Oceanography, 33, 104-114, 2020.

Fischer, H., Fundel, F., Ruth, U., Twarloh, B., Wegner, A., Udisti, R., Becagli, S., Castellano, E., Morganti, A., Severi, M., Wolff, E., Littot, G., Röthlisberger, R., Mulvaney, R., Hutterli, M. A., Kaufmann, P., Federer, U., Lambert, F., Bigler, M., Hansson, M., Jonsell, U., de Angelis, M., Boutron, C., Siggaard-Andersen, M.-L., Steffensen, J. P., Barbante, C., Gaspari, V., Gabrielli, P., and Wagenbach, D.: Reconstruction of millennial changes in dust emission, transport and regional sea ice coverage using the deep EPICA ice cores from the Atlantic and Indian Ocean sector of Antarctica, Earth and Planetary Science Letters, 260, 340-354, https://doi.org/10.1016/j.epsl.2007.06.014, 2007a.

Fischer, H., Fundel, F., Ruth, U., Twarloh, B., Wegner, A., Udisti, R., Becagli, S., Castellano, E., Morganti, A., Severi, M., Wolff, E. W., Littot, G. C., Röthlisberger, R., Mulvaney, R., Hutterli, M. A., Kaufmann, P. R., Federer, U., Lambert, F., Bigler, C., Hansson, M. E., Jonsell, U., de Angelis, M., Boutron, C. F., Siggaard-Andersen, M.-L., Steffensen, J. P., Barbante, C., Gaspari, V., Gabrielli, P., and

https://doi.org/10.5194/egusphere-2024-246
Preprint. Discussion started: 1 February 2024

Wagenbach, D.: EPICA EDML chemical concentrations and fluxes, PANGAEA [dataset], 10.1594/PANGAEA.683642, 2007b.

Geibert, W., Stimac, I., Rutgers Van Der Loeff, M., and Kuhn, G.: Dating Deep-Sea Sediments With 230Th Excess Using a Constant Rate of Supply Model, Paleoceanography and Paleoclimatology, 34, 1895-1912, https://doi.org/10.1029/2019PA003663, 2019.

Gersonde, R. and Zielinski, U.: The reconstruction of late Quaternary Antarctic sea-ice distribution—the use of diatoms as a proxy for sea-ice, Palaeogeography, Palaeoclimatology, Palaeoecology, 162, 263-286, https://doi.org/10.1016/S0031-0182(00)00131-0, 2000.

Gersonde, R., Crosta, X., Abelmann, A., and Armand, L.: Sea-surface temperature and sea ice distribution of the Southern Ocean at the EPILOG Last Glacial Maximum—a circum-Antarctic view based on siliceous microfossil records, Quaternary Science Reviews, 24, 869-896, https://doi.org/10.1016/j.quascirev.2004.07.015, 2005.

Gersonde, R., Abelmann, A., Brathauer, U., Becquey, S., Bianchi, C., Cortese, G., Grobe, H., Kuhn, G., Niebler, H.-S., Segl, M., Sieger, R., Zielinski, U., and Fütterer, D. K.: Last glacial sea surface temperatures and sea-ice extent in the Southern Ocean (Atlantic-Indian sector): A multiproxy approach, Paleoceanography, 18, https://doi.org/10.1029/2002PA000809, 2003.

Goelzer, H., Huybrechts, P., Loutre, M. F., and Fichefet, T.: Last Interglacial climate and sea-level evolution from a coupled ice sheet–climate model, Clim. Past, 12, 2195-2213, 10.5194/cp-12-2195-2016, 2016.

Gordon, A. L., Visbeck, M., and Huber, B.: Export of Weddell Sea deep and bottom water, Journal of Geophysical Research: Oceans, 106, 9005-9017, https://doi.org/10.1029/2000JC000281, 2001.

Greene, C. A., Young, D. A., Gwyther, D. E., Galton-Fenzi, B. K., and Blankenship, D. D.: Seasonal dynamics of Totten Ice Shelf controlled by sea ice buttressing, The Cryosphere, 12, 2869-2882, 10.5194/tc-12-2869-2018, 2018.

Hagemann, J. R., Lembke-Jene, L., Lamy, F., Vorrath, M. E., Kaiser, J., Müller, J., Arz, H. W., Hefter, J., Jaeschke, A., Ruggieri, N., and Tiedemann, R.: Upper-ocean temperature characteristics in the subantarctic southeastern Pacific based on biomarker reconstructions, Clim. Past, 19, 1825-1845, 10.5194/cp-19-1825-2023, 2023.

Hayes, C. T., Martínez-García, A., Hasenfratz, A. P., Jaccard, S. L., Hodell, D. A., Sigman, D. M., Haug, G. H., and Anderson, R. F.: A stagnation event in the deep South Atlantic during the last interglacial period, Science, 346, 1514-1517, doi:10.1126/science.1256620, 2014.

Hellmer, H. H.: Impact of Antarctic ice shelf basal melting on sea ice and deep ocean properties, Geophysical Research Letters, 31, https://doi.org/10.1029/2004GL019506, 2004.

Heroy, D. C., Sjunneskog, C., and Anderson, J. B.: Holocene climate change in the Bransfield Basin, Antarctic Peninsula: evidence from sediment and diatom analysis, Antarctic Science, 20, 69-87, 10.1017/S0954102007000788, 2008.

Herron, M. J. and Anderson, J. B.: Late quaternary glacial history of the South Orkney Plateau, Antarctica, Quaternary Research, 33, 265-275, https://doi.org/10.1016/0033-5894(90)90055-P, 1990.

Hibler, W. D.: A Dynamic Thermodynamic Sea Ice Model, Journal of Physical Oceanography, 9, 815-846, https://doi.org/10.1175/1520-0485(1979)009<0815:ADTSIM>2.0.CO;2, 1979.

Hoffman, J. S., Clark, P. U., Parnell, A. C., and He, F.: Regional and global sea-surface temperatures during the last interglaciation, Science, 355, 276-279, doi:10.1126/science.aai8464, 2017.

Holloway, M. D., Sime, L. C., Singarayer, J. S., Tindall, J. C., Bunch, P., and Valdes, P. J.: Antarctic last interglacial isotope peak in response to sea ice retreat not ice-sheet collapse, Nature Communications, 7, 12293, 10.1038/ncomms12293, 2016.

https://doi.org/10.5194/egusphere-2024-246
Preprint. Discussion started: 1 February 2024

Holloway, M. D., Sime, L. C., Allen, C. S., Hillenbrand, C. D., Bunch, P., Wolff, E., and Valdes, P. J.: The spatial structure of the 128 ka Antarctic sea ice minimum, Geophysical Research Letters, 44, 11,129-111,139, 10.1002/2017GL074594, 2017.

Hopmans, E. C., Weijers, J. W. H., Schefuß, E., Herfort, L., Sinninghe Damsté, J. S., and Schouten, S.: A novel proxy for terrestrial organic matter in sediments based on branched and isoprenoid tetraether lipids, Earth and Planetary Science Letters, 224, 107-116, https://doi.org/10.1016/j.epsl.2004.05.012, 2004.

Huhn, O., Hellmer, H. H., Rhein, M., Rodehacke, C., Roether, W., Schodlok, M. P., and Schröder, M.: Evidence of deep- and bottom-water formation in the western Weddell Sea, Deep Sea Research Part II: Topical Studies in Oceanography, 55, 1098-1116, https://doi.org/10.1016/j.dsr2.2007.12.015, 2008.

Inglis, G. N., Farnsworth, A., Lunt, D., Foster, G. L., Hollis, C. J., Pagani, M., Jardine, P. E., Pearson, P. N., Markwick, P., Galsworthy, A. M. J., Raynham, L., Taylor, K. W. R., and Pancost, R. D.: Descent toward the Icehouse: Eocene sea surface cooling inferred from GDGT distributions, Paleoceanography, 30, 1000-1020, https://doi.org/10.1002/2014PA002723, 2015.

Jacobs, S. S.: On the nature and significance of the Antarctic Slope Front, Marine Chemistry, 35, 9-24, https://doi.org/10.1016/S0304-4203(09)90005-6, 1991.

Johnson, R. G. and Andrews, J. T.: Glacial terminations in the oxygen isotope record of deep sea cores: hypothesis of massive Antarctic ice-shelf destruction, Palaeogeography, Palaeoclimatology, Palaeoecology, 53, 107-138, https://doi.org/10.1016/0031-0182(86)90041-6, 1986.

Joughin, I. and Alley, R. B.: Stability of the West Antarctic ice sheet in a warming world, Nature Geoscience, 4, 506-513, 10.1038/ngeo1194, 2011.

Jungclaus, J. H., Keenlyside, N., Botzet, M., Haak, H., Luo, J.-J., Latif, M., Marotzke, J., Mikolajewicz, U., and Roeckner, E.: Ocean Circulation and Tropical Variability in the Coupled Model ECHAM5/MPI-OM, Journal of Climate, 19, 3952-3972, https://doi.org/10.1175/JCLI3827.1, 2006.

Kim, J.-H., Crosta, X., Willmott, V., Renssen, H., Bonnin, J., Helmke, P., Schouten, S., and Sinninghe Damsté, J. S.: Holocene subsurface temperature variability in the eastern Antarctic continental margin, Geophysical Research Letters, 39, https://doi.org/10.1029/2012GL051157, 2012.

Kim, J.-H., van der Meer, J., Schouten, S., Helmke, P., Willmott, V., Sangiorgi, F., Koç, N., Hopmans, E. C., and Damsté, J. S. S.: New indices and calibrations derived from the distribution of crenarchaeal isoprenoid tetraether lipids: Implications for past sea surface temperature reconstructions, Geochimica et Cosmochimica Acta, 74, 4639-4654, https://doi.org/10.1016/j.gca.2010.05.027, 2010.

Lamping, N., Müller, J., Esper, O., Hillenbrand, C.-D., Smith, J. A., and Kuhn, G.: Highly branched isoprenoids reveal onset of deglaciation followed by dynamic sea-ice conditions in the western Amundsen Sea, Antarctica, Quaternary Science Reviews, 228, 106103, https://doi.org/10.1016/j.quascirev.2019.106103, 2020.

Lamping, N., Müller, J., Hefter, J., Mollenhauer, G., Haas, C., Shi, X., Vorrath, M. E., Lohmann, G., and Hillenbrand, C. D.: Evaluation of lipid biomarkers as proxies for sea ice and ocean temperatures along the Antarctic continental margin, Clim. Past, 17, 2305-2326, 10.5194/cp-17-2305-2021, 2021.

Lee, J. I., Bak, Y.-S., Yoo, K.-C., Lim, H. S., Yoon, H. I., and Yoon, S. H.: Climate changes in the South Orkney Plateau during the last 8600 years, The Holocene, 20, 395-404, 10.1177/0959683609353430, 2010.

Liu, X.-L., Summons, R. E., and Hinrichs, K.-U.: Extending the known range of glycerol ether lipids in the environment: structural assignments based on tandem mass spectral fragmentation patterns, Rapid Communications in Mass Spectrometry, 26, 2295-2302, https://doi.org/10.1002/rcm.6355, 2012a.

Liu, X.-L., Lipp, J. S., Simpson, J. H., Lin, Y.-S., Summons, R. E., and Hinrichs, K.-U.: Mono- and dihydroxyl glycerol dibiphytanyl glycerol tetraethers in marine sediments: Identification of both core and

https://doi.org/10.5194/egusphere-2024-246
Preprint. Discussion started: 1 February 2024

intact polar lipid forms, Geochimica et Cosmochimica Acta, 89, 102-115, https://doi.org/10.1016/j.gca.2012.04.053, 2012b.

Loveland, T. R., Reed, B. C., Brown, J. F., Ohlen, D. O., Zhu, Z., Yang, L., and Merchant, J. W.: Development of a global land cover characteristics database and IGBP DISCover from 1 km AVHRR data, International Journal of Remote Sensing, 21, 1303-1330, 10.1080/014311600210191, 2000.

Lü, X., Liu, X.-L., Elling, F. J., Yang, H., Xie, S., Song, J., Li, X., Yuan, H., Li, N., and Hinrichs, K.-U.: Hydroxylated isoprenoid GDGTs in Chinese coastal seas and their potential as a paleotemperature proxy for mid-to-low latitude marginal seas, Organic Geochemistry, 89-90, 31-43, https://doi.org/10.1016/j.orggeochem.2015.10.004, 2015.

Lunt, D. J., Abe-Ouchi, A., Bakker, P., Berger, A., Braconnot, P., Charbit, S., Fischer, N., Herold, N., Jungclaus, J. H., Khon, V. C., Krebs-Kanzow, U., Langebroek, P. M., Lohmann, G., Nisancioglu, K. H., Otto-Bliesner, B. L., Park, W., Pfeiffer, M., Phipps, S. J., Prange, M., Rachmayani, R., Renssen, H., Rosenbloom, N., Schneider, B., Stone, E. J., Takahashi, K., Wei, W., Yin, Q., and Zhang, Z. S.: A multi-model assessment of last interglacial temperatures, Clim. Past, 9, 699-717, 10.5194/cp-9-699-2013, 2013.

Marino, G., Rohling, E. J., Rodríguez-Sanz, L., Grant, K. M., Heslop, D., Roberts, A. P., Stanford, J. D., and Yu, J.: Bipolar seesaw control on last interglacial sea level, Nature, 522, 197-201, 10.1038/nature14499, 2015.

Marsland, S. J., Haak, H., Jungclaus, J. H., Latif, M., and Röske, F.: The Max-Planck-Institute global ocean/sea ice model with orthogonal curvilinear coordinates, Ocean Modelling, 5, 91-127, https://doi.org/10.1016/S1463-5003(02)00015-X, 2003.

Massé, G., Belt, S. T., Crosta, X., Schmidt, S., Snape, I., Thomas, D. N., and Rowland, S. J.: Highly branched isoprenoids as proxies for variable sea ice conditions in the Southern Ocean, Antarctic Science, 23, 487-498, 10.1017/S0954102011000381, 2011.

Massom, R. A., Scambos, T. A., Bennetts, L. G., Reid, P., Squire, V. A., and Stammerjohn, S. E.: Antarctic ice shelf disintegration triggered by sea ice loss and ocean swell, Nature, 558, 383-389, https://doi.org/10.1038/s41586-018-0212-1, 2018.

Masson-Delmotte, V., Buiron, D., Ekaykin, A., Frezzotti, M., Gallée, H., Jouzel, J., Krinner, G., Landais, A., Motoyama, H., Oerter, H., Pol, K., Pollard, D., Ritz, C., Schlosser, E., Sime, L. C., Sodemann, H., Stenni, B., Uemura, R., and Vimeux, F.: A comparison of the present and last interglacial periods in six Antarctic ice cores, Clim. Past, 7, 397-423, 10.5194/cp-7-397-2011, 2011.

Members, E.: One-to-one coupling of glacial climate variability in Greenland and Antarctica, Nature, 444, 195-198, 10.1038/nature05301, 2006.

Members, E.: Stable oxygen isotopes of ice core EDML, PANGAEA [dataset], 10.1594/PANGAEA.754444, 2010.

Mercer, J. H.: Antarctic ice and Sangamon sea level, 1968.

Michalchuk, B. R., Anderson, J. B., Wellner, J. S., Manley, P. L., Majewski, W., and Bohaty, S.: Holocene climate and glacial history of the northeastern Antarctic Peninsula: the marine sedimentary record from a long SHALDRIL core, Quaternary Science Reviews, 28, 3049-3065, https://doi.org/10.1016/j.quascirev.2009.08.012, 2009.

Morozov, E. G., Frey, D. I., and Tarakanov, R. Y.: Antarctic Bottom Water Flow through the Eastern Part of the Philip Passage in the Weddell Sea, Oceanology, 60, 589-592, 10.1134/S000143702005015X, 2020.

Müller, J., Wagner, A., Fahl, K., Stein, R., Prange, M., and Lohmann, G.: Towards quantitative sea ice reconstructions in the northern North Atlantic: A combined biomarker and numerical modelling approach, Earth and Planetary Science Letters, 306, 137-148, https://doi.org/10.1016/j.epsl.2011.04.011, 2011.

Müller, P. J. and Schneider, R.: An automated leaching method for the determination of opal in sediments and particulate matter, Deep Sea Research Part I: Oceanographic Research Papers, 40, 425-444, 1993.

Naughten, K. A., Meissner, K. J., Galton-Fenzi, B. K., England, M. H., Timmermann, R., Hellmer, H. H., Hattermann, T., and Debernard, J. B.: Intercomparison of Antarctic ice-shelf, ocean, and sea-ice interactions simulated by MetROMS-iceshelf and FESOM 1.4, Geosci. Model Dev., 11, 1257-1292, 10.5194/gmd-11-1257-2018, 2018.

Naveira Garabato, A. C., McDonagh, E. L., Stevens, D. P., Heywood, K. J., and Sanders, R. J.: On the export of Antarctic Bottom Water from the Weddell Sea, Deep Sea Research Part II: Topical Studies in Oceanography, 49, 4715-4742, https://doi.org/10.1016/S0967-0645(02)00156-X, 2002.

Ó Cofaigh, C., Davies, B. J., Livingstone, S. J., Smith, J. A., Johnson, J. S., Hocking, E. P., Hodgson, D. A., Anderson, J. B., Bentley, M. J., Canals, M., Domack, E., Dowdeswell, J. A., Evans, J., Glasser, N. F., Hillenbrand, C.-D., Larter, R. D., Roberts, S. J., and Simms, A. R.: Reconstruction of ice-sheet changes in the Antarctic Peninsula since the Last Glacial Maximum, Quaternary Science Reviews, 100, 87-110, https://doi.org/10.1016/j.quascirev.2014.06.023, 2014.

Olbers, D., Gouretsky, V., Seiss, G., and Schröter, J.: Hydrographic atlas of the Southern Ocean, Alfred-Wegener-Institut, Bremerhaven1992.

Orsi, A. H., Johnson, G. C., and Bullister, J. L.: Circulation, mixing, and production of Antarctic Bottom Water, Progress in Oceanography, 43, 55-109, https://doi.org/10.1016/S0079-6611(99)00004-X, 1999.

Orsi, A. H., Nowlin, W. D., and Whitworth, T.: On the circulation and stratification of the Weddell Gyre, Deep Sea Research Part I: Oceanographic Research Papers, 40, 169-203, https://doi.org/10.1016/0967-0637(93)90060-G, 1993.

Orsi, A. H., Whitworth, T., and Nowlin, W. D.: On the meridional extent and fronts of the Antarctic Circumpolar Current, Deep Sea Research Part I: Oceanographic Research Papers, 42, 641-673, https://doi.org/10.1016/0967-0637(95)00021-W, 1995.

Otto-Bliesner, B. L., Rosenbloom, N., Stone, E. J., McKay, N. P., Lunt, D. J., Brady, E. C., and Overpeck, J. T.: How warm was the last interglacial? New model–data comparisons, Philosophical Transactions of the Royal Society A: Mathematical, Physical and Engineering Sciences, 371, 20130097, doi:10.1098/rsta.2013.0097, 2013.

Pedro, J. B., van Ommen, T. D., Rasmussen, S. O., Morgan, V. I., Chappellaz, J., Moy, A. D., Masson-Delmotte, V., and Delmotte, M.: The last deglaciation: timing the bipolar seesaw, Clim. Past, 7, 671-683, 10.5194/cp-7-671-2011, 2011.

Pedro, J. B., Bostock, H. C., Bitz, C. M., He, F., Vandergoes, M. J., Steig, E. J., Chase, B. M., Krause, C. E., Rasmussen, S. O., Markle, B. R., and Cortese, G.: The spatial extent and dynamics of the Antarctic Cold Reversal, Nature Geoscience, 9, 51-55, 10.1038/ngeo2580, 2016.

Pellichero, V., Sallée, J.-B., Chapman, C. C., and Downes, S. M.: The southern ocean meridional overturning in the sea-ice sector is driven by freshwater fluxes, Nature Communications, 9, 1789, 10.1038/s41467-018-04101-2, 2018.

Pollard, D. and DeConto, R. M.: Modelling West Antarctic ice sheet growth and collapse through the past five million years, Nature, 458, 329-332, 2009.

Raddatz, T. J., Reick, C. H., Knorr, W., Kattge, J., Roeckner, E., Schnur, R., Schnitzler, K. G., Wetzel, P., and Jungclaus, J.: Will the tropical land biosphere dominate the climate–carbon cycle feedback during the twenty-first century?, Climate Dynamics, 29, 565-574, 10.1007/s00382-007-0247-8, 2007.

https://doi.org/10.5194/egusphere-2024-246
Preprint. Discussion started: 1 February 2024

Renssen, H., Goosse, H., Fichefet, T., Masson-Delmotte, V., and Koç, N.: Holocene climate evolution in the high-latitude Southern Hemisphere simulated by a coupled atmosphere-sea ice-ocean-vegetation model, The Holocene, 15, 951-964, 10.1191/0959683605hl869ra, 2005.

Reynolds, R. W., Rayner, N. A., Smith, T. M., Stokes, D. C., and Wang, W.: An Improved In Situ and Satellite SST Analysis for Climate, Journal of Climate, 15, 1609-1625, https://doi.org/10.1175/1520-0442(2002)015<1609:AIISAS>2.0.CO;2, 2002.

Reynolds, R. W., Smith, T. M., Liu, C., Chelton, D. B., Casey, K. S., and Schlax, M. G.: Daily High-Resolution-Blended Analyses for Sea Surface Temperature, Journal of Climate, 20, 5473-5496, https://doi.org/10.1175/2007JCLI1824.1, 2007.

Rhodes, R., Kohfeld, K., Bostock, H., Crosta, X., Leventer, A., Meissner, K., and Esper, O.: Understanding past changes in sea ice in the Southern Ocean, Past Global Changes Magazine, 27(1), 31, https://doi.org/10.22498/pages.27.1.31, 2019.

Riaux-Gobin, C. and Poulin, M.: Possible symbiosis of Berkeleya adeliensis Medlin, Synedropsis fragilis (Manguin) Hasle et al. and Nitzschia lecointei Van Heurck (Bacillariophyta) associated with land-fast ice in Adélie Land, Antarctica, Diatom Research, 19, 265-274, 2004.

Rintoul, S. R.: The global influence of localized dynamics in the Southern Ocean, Nature, 558, 209-218, https://doi.org/10.1038/s41586-018-0182-3, 2018.

Robel, A. A.: Thinning sea ice weakens buttressing force of iceberg mélange and promotes calving, Nature Communications, 8, 14596, 10.1038/ncomms14596, 2017.

Ryves, D. B., Battarbee, R. W., and Fritz, S. C.: The dilemma of disappearing diatoms: Incorporating diatom dissolution data into palaeoenvironmental modelling and reconstruction, Quaternary Science Reviews, 28, 120-136, https://doi.org/10.1016/j.quascirev.2008.08.021, 2009.

Sadatzki, H., Opdyke, B., Menviel, L., Leventer, A., Hope, J. M., Brocks, J. J., Fallon, S., Post, A. L., O'Brien, P. E., Grant, K., and Armand, L.: Early sea ice decline off East Antarctica at the last glacial–interglacial climate transition, Science Advances, 9, eadh9513, doi:10.1126/sciadv.adh9513, 2023.

Seabrooke, J. M., Hufford, G. L., and Elder, R. B.: Formation of Antarctic bottom water in the Weddell Sea, Journal of Geophysical Research (1896-1977), 76, 2164-2178, https://doi.org/10.1029/JC076i009p02164, 1971.

Shevenell, A. E., Domack, E. W., and Kernan, G. M.: Record of Holocene palaeoclimate change along the Antarctic Peninsula: evidence from glacial marine sediments, Lallemand Fjord, Papers and Proceedings of the Royal Society of Tasmania, 55-64,

Smik, L., Belt, S. T., Lieser, J. L., Armand, L. K., and Leventer, A.: Distributions of highly branched isoprenoid alkenes and other algal lipids in surface waters from East Antarctica: Further insights for biomarker-based paleo sea-ice reconstruction, Organic Geochemistry, 95, 71-80, https://doi.org/10.1016/j.orggeochem.2016.02.011, 2016.

Steig, E. J., Huybers, K., Singh, H. A., Steiger, N. J., Ding, Q., Frierson, D. M. W., Popp, T., and White, J. W. C.: Influence of West Antarctic Ice Sheet collapse on Antarctic surface climate, Geophysical Research Letters, 42, 4862-4868, https://doi.org/10.1002/2015GL063861, 2015.

Stepanek, C., Samakinwa, E., Knorr, G., and Lohmann, G.: Contribution of the coupled atmosphere–ocean–sea ice–vegetation model COSMOS to the PlioMIP2, Clim. Past, 16, 2275-2323, 10.5194/cp-16-2275-2020, 2020.

Stevens, B., Giorgetta, M., Esch, M., Mauritsen, T., Crueger, T., Rast, S., Salzmann, M., Schmidt, H., Bader, J., Block, K., Brokopf, R., Fast, I., Kinne, S., Kornblueh, L., Lohmann, U., Pincus, R., Reichler, T., and Roeckner, E.: Atmospheric component of the MPI-M Earth System Model: ECHAM6, Journal of Advances in Modeling Earth Systems, 5, 146-172, https://doi.org/10.1002/jame.20015, 2013.

https://doi.org/10.5194/egusphere-2024-246
Preprint. Discussion started: 1 February 2024

Sutter, J., Gierz, P., Grosfeld, K., Thoma, M., and Lohmann, G.: Ocean temperature thresholds for Last Interglacial West Antarctic Ice Sheet collapse, Geophysical Research Letters, 43, 2675-2682, https://doi.org/10.1002/2016GL067818, 2016.

Taylor, F. and Sjunneskog, C.: Postglacial marine diatom record of the Palmer Deep, Antarctic Peninsula (ODP Leg 178, Site 1098) 2. Diatom assemblages, Paleoceanography, 17, PAL 2-1-PAL 2-12, https://doi.org/10.1029/2000PA000564, 2002.

Taylor, F., Whitehead, J., and Domack, E.: Holocene paleoclimate change in the Antarctic Peninsula: evidence from the diatom, sedimentary and geochemical record, Marine Micropaleontology, 41, 25-43, https://doi.org/10.1016/S0377-8398(00)00049-9, 2001.

Thompson, A. F., Stewart, A. L., Spence, P., and Heywood, K. J.: The Antarctic Slope Current in a Changing Climate, Reviews of Geophysics, 56, 741-770, https://doi.org/10.1029/2018RG000624, 2018.

Turney, C. S. M., Fogwill, C. J., Golledge, N. R., McKay, N. P., van Sebille, E., Jones, R. T., Etheridge, D., Rubino, M., Thornton, D. P., Davies, S. M., Ramsey, C. B., Thomas, Z. A., Bird, M. I., Munksgaard, N. C., Kohno, M., Woodward, J., Winter, K., Weyrich, L. S., Rootes, C. M., Millman, H., Albert, P. G., Rivera, A., van Ommen, T., Curran, M., Moy, A., Rahmstorf, S., Kawamura, K., Hillenbrand, C.-D., Weber, M. E., Manning, C. J., Young, J., and Cooper, A.: Early Last Interglacial ocean warming drove substantial ice mass loss from Antarctica, Proceedings of the National Academy of Sciences, 117, 3996-4006, doi:10.1073/pnas.1902469117, 2020.

Vaughan, D. G., Comiso, J. C., Allison, I., Carrasco, J., Kaser, G., Kwok, R., Mote, P., Murray, T., Paul, F., Ren, J., Rigno, E., Solomina, O., Steffen, K., and Zhang, T.: Observations: Cryosphere, Cambridge University Press, Cambridge, United Kingdom and New York, NY, USA, 2013.

Vernet, M., Geibert, W., Hoppema, M., Brown, P. J., Haas, C., Hellmer, H. H., Jokat, W., Jullion, L., Mazloff, M., Bakker, D. C. E., Brearley, J. A., Croot, P., Hattermann, T., Hauck, J., Hillenbrand, C.-D., Hoppe, C. J. M., Huhn, O., Koch, B. P., Lechtenfeld, O. J., Meredith, M. P., Naveira Garabato, A. C., Nöthig, E.-M., Peeken, I., Rutgers van der Loeff, M. M., Schmidtko, S., Schröder, M., Strass, V. H., Torres-Valdés, S., and Verdy, A.: The Weddell Gyre, Southern Ocean: Present Knowledge and Future Challenges, Reviews of Geophysics, 57, 623-708, https://doi.org/10.1029/2018RG000604, 2019.

Viseras, C. and Maldonado, A.: Facies architecture, seismic stratigraphy and development of a high-latitude basin: the Powell Basin (Antarctica), Marine Geology, 157, 69-87, https://doi.org/10.1016/S0025-3227(98)00136-4, 1999.

Vorrath, M. E., Müller, J., Esper, O., Mollenhauer, G., Haas, C., Schefuß, E., and Fahl, K.: Highly branched isoprenoids for Southern Ocean sea ice reconstructions: a pilot study from the Western Antarctic Peninsula, Biogeosciences, 16, 2961-2981, 10.5194/bg-16-2961-2019, 2019.

Vorrath, M. E., Müller, J., Rebolledo, L., Cárdenas, P., Shi, X., Esper, O., Opel, T., Geibert, W., Muñoz, P., Haas, C., Kuhn, G., Lange, C. B., Lohmann, G., and Mollenhauer, G.: Sea ice dynamics in the Bransfield Strait, Antarctic Peninsula, during the past 240 years: a multi-proxy intercomparison study, Clim. Past, 16, 2459-2483, 10.5194/cp-16-2459-2020, 2020.

Vorrath, M. E., Müller, J., Cárdenas, P., Opel, T., Mieruch, S., Esper, O., Lembke-Jene, L., Etourneau, J., Vieth-Hillebrand, A., Lahajnar, N., Lange, C. B., Leventer, A., Evangelinos, D., Escutia, C., and Mollenhauer, G.: Deglacial and Holocene sea-ice and climate dynamics in the Bransfield Strait, northern Antarctic Peninsula, Clim. Past, 19, 1061-1079, 10.5194/cp-19-1061-2023, 2023.

Waelbroeck, C., Skinner, L. C., Labeyrie, L., Duplessy, J.-C., Michel, E., Vazquez Riveiros, N., Gherardi, J.-M., and Dewilde, F.: The timing of deglacial circulation changes in the Atlantic, Paleoceanography, 26, https://doi.org/10.1029/2010PA002007, 2011.

Watson, A. J., Vallis, G. K., and Nikurashin, M.: Southern Ocean buoyancy forcing of ocean ventilation and glacial atmospheric CO2, Nature Geoscience, 8, 861-864, 10.1038/ngeo2538, 2015.

Weber, M. E., Bailey, I., Hemming, S. R., Martos, Y. M., Reilly, B. T., Ronge, T. A., Brachfeld, S., Williams, T., Raymo, M., Belt, S. T., Smik, L., Vogel, H., Peck, V. L., Armbrecht, L., Cage, A., Cardillo, F. G., Du, Z., Fauth, G., Fogwill, C. J., Garcia, M., Garnsworthy, M., Glüder, A., Guitard, M., Gutjahr, M., Hernández-Almeida, I., Hoem, F. S., Hwang, J.-H., Iizuka, M., Kato, Y., Kenlee, B., Oconnell, S., Pérez, L. F., Seki, O., Stevens, L., Tauxe, L., Tripathi, S., Warnock, J., and Zheng, X.: Antiphased dust deposition and productivity in the Antarctic Zone over 1.5 million years, Nature Communications, 13, 2044, 10.1038/s41467-022-29642-5, 2022.

Wei, W. and Lohmann, G.: Simulated Atlantic Multidecadal Oscillation during the Holocene, Journal of Climate, 25, 6989-7002, https://doi.org/10.1175/JCLI-D-11-00667.1, 2012.

Williams, T. J., Martin, E. E., Sikes, E., Starr, A., Umling, N. E., and Glaubke, R.: Neodymium isotope evidence for coupled Southern Ocean circulation and Antarctic climate throughout the last 118,000 years, Quaternary Science Reviews, 260, 106915, https://doi.org/10.1016/j.quascirev.2021.106915, 2021.

Xiao, W., Esper, O., and Gersonde, R.: Last Glacial - Holocene climate variability in the Atlantic sector of the Southern Ocean, Quaternary Science Reviews, 135, 115-137, https://doi.org/10.1016/j.quascirev.2016.01.023, 2016a.

Xiao, W., Frederichs, T., Gersonde, R., Kuhn, G., Esper, O., and Zhang, X.: Constraining the dating of late Quaternary marine sediment records from the Scotia Sea (Southern Ocean), Quaternary Geochronology, 31, 97-118, https://doi.org/10.1016/j.quageo.2015.11.003, 2016b.

Xiao, W., Xu, Y., Zhang, C., Lin, J., Wu, W., Lü, X., Tan, J., Zhang, X., Zheng, F., Song, X., Zhu, Y., Yang, Y., Zhang, H., Wenzhöfer, F., Rowden, A. A., and Glud, R. N.: Disentangling Effects of Sea Surface Temperature and Water Depth on Hydroxylated Isoprenoid GDGTs: Insights From the Hadal Zone and Global Sediments, Geophysical Research Letters, 50, e2023GL103109, https://doi.org/10.1029/2023GL103109, 2023.

Zhang, X., Lohmann, G., Knorr, G., and Xu, X.: Different ocean states and transient characteristics in Last Glacial Maximum simulations and implications for deglaciation, Clim. Past, 9, 2319-2333, 10.5194/cp-9-2319-2013, 2013.

Zhang, Y. G., Pagani, M., and Wang, Z.: Ring Index: A new strategy to evaluate the integrity of TEX86 paleothermometry, Paleoceanography, 31, 220-232, https://doi.org/10.1002/2015PA002848, 2016.

Zielinski, U. and Gersonde, R.: Diatom distribution in Southern Ocean surface sediments (Atlantic sector): Implications for paleoenvironmental reconstructions, Palaeogeography, Palaeoclimatology, Palaeoecology, 129, 213-250, https://doi.org/10.1016/S0031-0182(96)00130-7, 1997.